BJGEO

Brazilian Journal of Geology

Geochemistry and U-Pb geochronology of columbite of the Cachoeirinha Deposit, Rondônia Tin Province, Brazil

Raquel Guimarães da Silva[1]* ⓘ, Valmir da Silva Souza[1] ⓘ, Guilherme de Oliveira Gonçalves[1] ⓘ,
Luiza dos Santos Ferreira[1] ⓘ, Paulo Sérgio Mendes dos Santos Júnior[2] ⓘ

Abstract

The Cachoeirinha Sn ± (Nb-Ta) deposit is an important producer of the Rondônia Tin Province. It is inserted in the regional unit named Rondônia Intrusive Suite (995–956 Ma) and hosts granular accumulations of columbite group minerals (CGM) embedded in thick Cenozoic colluvial-alluvial covers. Cachoeirinha CGM have subrounded to angular grains, with irregular to regular internal zoning, micro-inclusion, and exsolution features. They have columbite-(Fe) as the dominant mineral phase, with variation in the Ta/(Ta+Nb) ratio and with Sn, Ti, W, U, Ba, Cr, REE, and V as chemical impurities. It has high total REE content (LREE$_N$ depleted, HREE$_N$ enriched, Ce and Eu anomalies), $\delta^{18}O$ = 2.78‰, and with two U-Pb age groups: 1052 ± 6 and 909 ± 7 Ma. This information indicates that physicochemical oscillations favored the ionic substitutions and resorption mechanisms between Nb ↔ Ta, as well as coupled substitutions with the entry of geochemical impurities, according to the equation: 3(Sn, Ti, U, Si)$^{4+}$ + (W, Cr)$^{6+}$ ↔ 2(V, Nb, Ta)$^{5+}$ + 2(Al, REE)$^{3+}$ + (Fe, Mn, Ba)$^{2+}$, at the temperature range between 400° and 500°C. Finally, the Cachoeirinha Sn ± (Nb-Ta) alluvial deposit host ore is related to at least two Neo-Mesoproterozoic magmatic pulses.

KEYWORDS: Cachoeirinha Sn ± (Nb-Ta) deposit; Rondônia Tin Province; mineral chemistry; oxygen isotope; columbite U-Pb geochronology.

INTRODUCTION

The Rondônia Tin Province is located in the southwestern portion of the Amazonian craton, northern region of Brazil (Fig. 1). It is formed by Meso- to Neoproterozoic A-type rapakivi magmatic association, showing within-plate to post-collisional geochemical signature, and emplaced during successive episodes occurred between 1606 and 956 Ma (Kloosterman 1968, Priem *et al.* 1971, Leal *et al.* 1978, Isotta *et al.* 1978, Bettencourt *et al.* 1999, CPRM 2007). However, the most significant metal concentrations (Sn, W, Nb, and Ta), as well as F and some gems, are associated with the last three magmatic episodes that occurred between 1314 and 956 Ma. These primary ore concentrations are associated with the granitic cupolas, typically encapsulated in greisen, veins-veinlet, breccia, and small pegmatite bodies (Leite Jr. 2002, Bettencourt *et al.* 2005, Souza 2003, Sparrenberg 2003, Nascimento & Souza 2017). Nevertheless, voluminous secondary ore concentrations also occur in Plio-Pleistocene colluvial-alluvial covers, formed from the erosive disaggregation of the granitic cupolas (Veiga 1990, Souza 2003, CPRM 2007). Cassiterite, wolframite,

and columbite-tantalite are the main ore minerals exploited in the Rondônia Tin Province, often using an artisanal mining method called "garimpo" in Brazil (Dall'Igna 1996, Dall'Igna & Adamy 2010).

Cassiterite, wolframite, and columbite-tantalite typically exhibit chemical variations, internal zoning, intergrowths, exsolution, and mineral micro-inclusions as a result of changes in physicochemical parameters (pH, Eh, fO$_2$, temperature, and pressure) during nucleation and mineral growth in the magmatic-hydrothermal system (Jackson & Helgeson 1985, Černý *et al.* 1986, Möller *et al.* 1988, Černý & Ercit 1989, Heinrich 1990, Heinrich *et al.* 1996, Abdalla *et al.* 1998). Studies on variations in chemical and isotopic compositions of ore minerals of the Rondônia Tin Province are still insufficient or non-existent (*e.g.*, Souza & Botelho 2009, Nascimento & Souza 2017). In this paper, we present unprecedented data on mineralogical features (zonation, exsolution, and mineral intergrowth), mineral chemistry, oxygen isotope ($\delta^{18}O$), and U-Pb geochronology data of columbite group minerals (CGM) of the Cachoeirinha Sn ± (Nb-Ta) alluvial deposit. This set of information will assist in the mineralogical characterization of the CGM and contribute to determining the age and fingerprint of the Nb-Ta mineralization in the Rondônia Tin Province.

GEOLOGICAL AND METALLOGENETIC SETTING

The Meso- to Neoproterozoic A-type rapakivi magmatism at the Rondônia Tin Province occur intruded in the Paleoproterozoic basement rocks, represented by the regional

[1]Geosciences Institute, Universidade de Brasília – Brasília (DF), Brazil.
E-mails: raquelguimaraes123@gmail.com, valmirsouzaunb@gmail.com, guilherme.goncalves@unb.br, luiza.sferreiraa@gmail.com
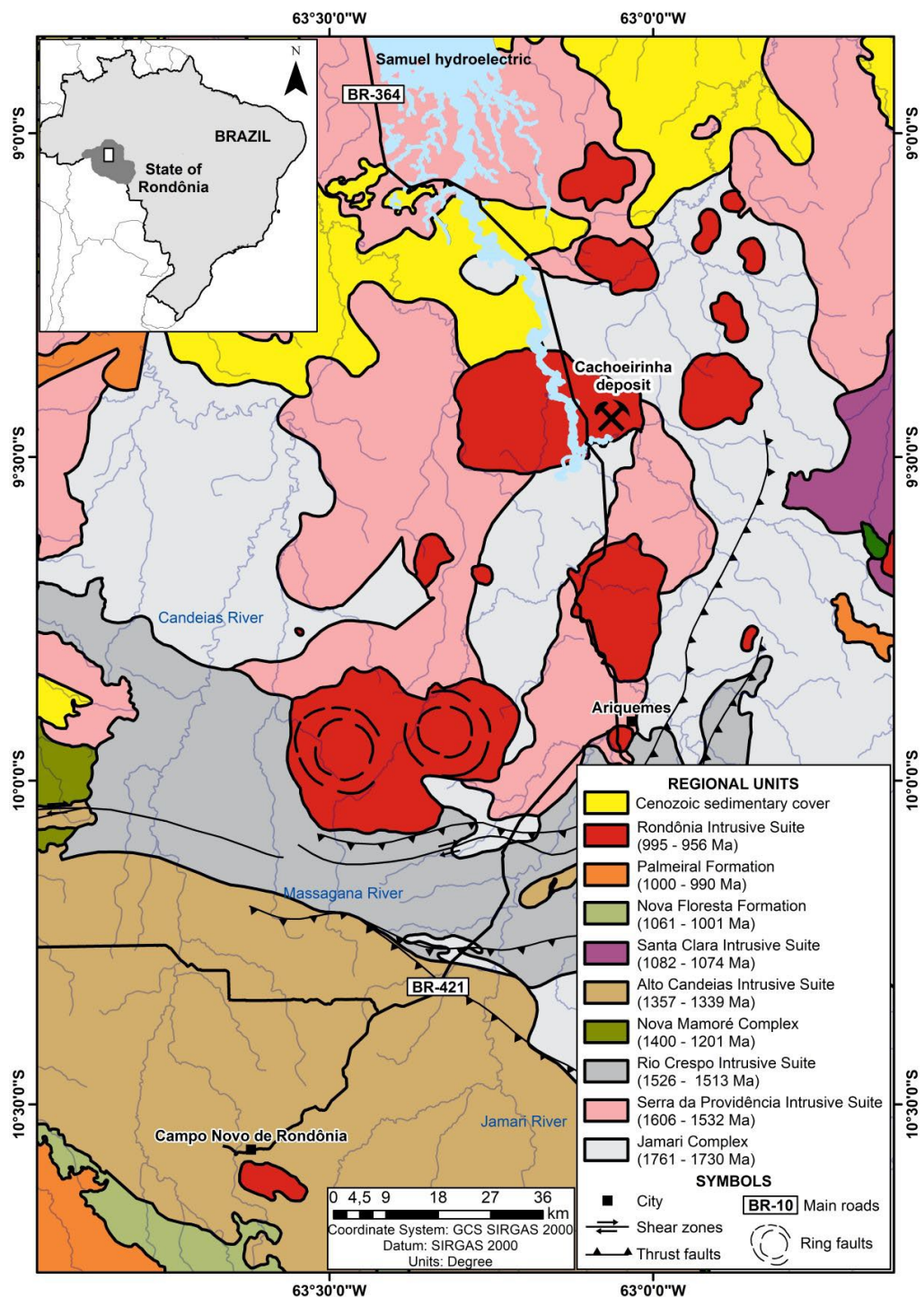
[2]Secretary of Environmental Development of the State of Rondônia – Porto Velho (RO), Brazil. E-mail: geopaulosergio@gmail.com

*Corresponding author.

Source: modified from CPRM (2007).

Figure 1. Simplified geological setting of the central-northern portion of the Rondônia Tin Province. Note the location indication of the Sn ± (Nb-Ta) Cachoeirinha deposit.

unit named Jamari Complex (Fig. 1). This basement unit brings together a variety of polydeformed medium to high-grade ortho- and paragneisses, migmatites, and charnoender-bitic associations, marked by successive tectonometamorphic events at 1.33–1.32 and 1.2–1.1 Ga (Isotta *et al.* 1978, Payolla *et al.* 2002, Souza et al. 2006, CPRM 2007, Santos *et al.* 2008, Bettencourt *et al.* 2010, Scandolara *et al.* 2013). On the contrary, the A-type rapakivi magmatism is formed by regional geological units to follow: Serra da Providência (1606–1532 Ma), Santo Antônio (1406 Ma), Teotônio (1387 Ma), Alto Candeias (1346–1338 Ma), São Lourenço–Caripunas (1314–1309 Ma),

Santa Clara (1082–1074 Ma), and Rondônia (995–956 Ma) intrusive suites. These magmatic suites are polyphasic stocks and batholiths, composed of medium to coarse rapakivi gran-ites (pyterlites and wiborgites), inequigranular syenogranites, monzogranites, and alkali-feldspar granites, with a smaller volume of porphyritic subvolcanic and volcanic rocks (micro-granite, albite granite, syenite, rhyolite, trachyte, and others). In general, these magmatic suites have alkaline to subalkaline, metaluminous to peraluminous composition, and within-plate to post-collisional geochemical signatures (Souza *et al.* 1975, Isotta *et al.* 1978, Leal *et al.* 1978, Bettencourt *et al.* 1999, 2010,

CPRM 2007, Santos *et al.* 2008). However, the most significant polymetallic concentrations are associated with the last three magmatic pulses, which occurred between 1314 and 974 Ma, represented by the regional units São Lourenço-Caripunas, Santa Clara, and Rondônia intrusive suites (Kloosterman 1966, 1967, Priem *et al.* 1971, Bettencourt *et al.* 1999, CPRM 2007).

The Cachoeirinha Sn ± (Nb-Ta) deposit is inserted in the Rondônia Intrusive Suite, which occurs mainly in the north-central portion of the State of Rondônia (Fig. 1). This regional unit often hosts ring-fault structures related to the polyphasic nature of the volcano-plutonic systems. The Rondônia Intrusive Suite encompasses a variety of lithologies: amphibole–biotite and alkali–feldspar syenogranite, syenite, and microsyenite, as well as rhyolite, trachyte, and rare rocks such as topaz Li–mica albite granite and topaz-quartz-feldspar porphyry granite (Priem *et al.* 1971, Bettencourt *et al.* 1999, 2005, Leite Jr. 2002, Souza 2003, Sparrenberger 2003, CPRM 2007). The primary mineralization sites are related to late magmatic to magmatic-hydrothermal stages, developed at the granitic cupola zones and surrounding wall rocks, with ore minerals normally encapsulated in endo- and exogreisen, vein-veinlet, breccia, and small pegmatite bodies (Yokoi *et al.* 1987, Leite Jr. 2002, Souza 2003, Sparrenberger 2003, Bettencourt *et al.* 2005, Nascimento & Souza 2017). Furthermore, the Plio-Pleistocene to Holocene erosive process on the granitic cupola zone favored the formation of important secondary metal concentrations along the alluvial or paleo-placer deposits (Bettencourt *et al.* 1988, Veiga *et al.* 1988, Veiga 1990, Oliveira & Valente 1993, Souza 2003).

Greisen and vein-veinlet are the most prominent mineralization sites. Greisen has an isotropic fabric with inequigranular medium- to coarse-grained, composed mainly of quartz, topaz, Li-F mica, fluorite, and phengite distributed in various proportions. Cassiterite, wolframite, columbite-tantalite, siderite, monazite, xenotime, thorite, titanite, scheelite, ilmenite, hematite, hollandite, chalcopyrite, pyrite, sphalerite, pyrrhotite, galena, bismuthinite, and molybdenite are some of the most common accessory minerals, as well as rare and exotic Ag and Bi-Te sulfides (Yokoi *et al.* 1987, Leite Jr. 2002, Souza 2003, Sparrenberger 2003, Nascimento & Souza 2017). Vein-veinlet usually form an interlaced set of subvertical tensile fractures extending from across the greisenized granitic cupola to the basement rocks. They present varied thicknesses, inequigranular medium- to coarse-grained textures and have quartz, topaz, and Li-F mica as main minerals. Cassiterite, wolframite, columbite-tantalite, fluorite, siderite, hematite, barite, sphalerite, arsenopyrite, chalcopyrite, and pyrite are the main accessory minerals (Souza 2003, Sparrenberger 2003, Santos Jr. 2015, Nascimento & Souza 2017). The alluvial or paleo-placer deposits are distributed around or directly above the primary mineralization sites (Figs. 2A and 2B), usually marked by planar to trough cross-stratification type sedimentary structures.

Figure 2. (A and B) Overview of the open pit mining of the alluvial Cachoeirinha deposit. (C) Ore concentration equipment gravitational used in Cachoeirinha open pit mining. (D) Bag with ore concentrate for subsequent transport and trade steps.

The geochemical and isotopic data presented in this paper come from columbite-tantalite concentrates from the open pit mining of the Cachoeirinha deposit (Figs. 2C and 2D). These concentrates are associated with thick alluvial or paleoplacer deposits, which are found near or overlay the primary mineralization sites. This deposit has been responsible for a significant portion of Nb-Ta production in the Rondônia Tin Province, which amounted to approximately 9,000 tons/ore in the year 2020 (ANM 2020).

ANALYTICAL PROCEDURES

The conventional petrography and scanning electron microscopy, mineral-chemistry, and U-Pb geochronology analytical procedures were carried out at the Geoscience Institute, Universidade de Brasilia (IG-UnB), Brazil. Oxygen isotope ($\delta^{18}O$) analysis was carried out at Queens University, applying the purest possible mineral samples previously separated in Brazil.

Conventional petrography and electron microscopy investigations were performed on four polished sections containing columbite-tantalite granular concentrates. A FEI QUANTA 450 model, with Chroma C2L *cathodoluminescence* imaging system and EDAX DigiView electron backscatter diffraction (EBSD) camera, was used. A focal distance of 10 mm for 10–20 s of clock time, with a probe between 0.1 and 0.2 nm, beam current of 400–500 pA, and an accelerating voltage of 20 kV were the analytical conditions applied. For electron-probe microanalyses (EPMA), a JEOL JXA-8230 model microanalyzer with five coupled wavelength dispersive spectrometers (WDS) was used. The analytical conditions consisted of an accelerating voltage of 20 kV, a beam current of 40 nA, a beam diameter of 1–2 μm, and counting times of 15 and 10 s for peak and background positions, respectively. The data reduction was performed with the ZAF program applying the specific standards of CGM.

Some trace elements and rare earth element (REE) compositions, as well as the U-Pb isotopic ratios, were measured using a Thermo Finnigan Element XR high-resolution single-collector sector field ICP-MS coupled to a 193-nm Iridia laser ablation system. The laser ablation system is equipped with a Cobalt tube cell chamber. The following masses were analyzed: ^{139}La, ^{140}Ce, ^{141}Pr, ^{143}Nd, ^{147}Sm, ^{151}Eu, ^{157}Gd, ^{159}Tb, ^{163}Dy, ^{165}Ho, ^{166}Er, ^{169}Tm, ^{172}Yb, ^{175}Lu, ^{177}Hf, ^{206}Pb, ^{232}Th, and ^{238}U. The laser parameters included an ablation spot size of 40 μm, a laser fluence of 2.0 J/cm², and a laser repetition rate of 20 Hz. Each spot analysis consisted of 20 s sample ablation and 10 s of background measurement. Each spot was placed next to or on top of the U-Pb spot analysis. The primary reference material was the NIST-612 glass (Jochum *et al.* 2016), and the reference materials used for quality control were the NIST-610 glass (Jochum *et al.* 2016) and Diamantina monazite (Gonçalves *et al.* 2018). The results were processed on Iolite 4.0 (Paton *et al.* 2011) as time-resolved signals and individual signal inspection was done with the assistance of the VizualAge (Petrus & Kamber 2012). The internal reference value used for calibration was a mean concentration of Ta_2O_5 previously measured by EPMA (10 wt%; Table 1). The precision of multiple analyses of quality control reference material is better than 5% for most elements and agrees with uncertainty with published data from Gonçalves *et al.* (2018) and Jochum *et al.* (2016). We also used a matrix-unmatched approach, i.e., using zircon as a calibrant. Therefore, data were normalized to the GJ-1 zircon (Jackson *et al.* 2004, Horstwood *et al.* 2016), and the 91500 (Wiedenbeck *et al.* 1995) and Plešovice zircon (Sláma *et al.* 2008, Horstwood *et al.* 2016) were used for quality control. The results obtained for the 91500 and Plešovice zircons are 1058 ± 5 Ma (2 s, n = 12, MSWD = 1.3) and 338 ± 1 Ma (2 s, n = 12, MSWD = 1.5), respectively. These results are within uncertainty of their reference values and attest to the accuracy and precision of the analytical round. Systematic uncertainty of ca. 1% is propagated on each final age. No common lead correction was applied and the ages are quoted at 2 s.

The isotopic $\delta^{18}O$ analysis was performed at Queen's Facility for Isotope Research (QFIR) in Kingston (Canada). The mineral sample preparation (columbite-tantalite) followed the method of Clayton and Mayeda (1963), utilizing bromine pentafluoride (BrF_5) and 5 mg of each sample in a silicate line for CO_2 extraction. After purging the line with Ar, BrF_5 was added to each sample in individual steel bombs, heated at 550–600°C for 8 h. This liberated the oxygen from the crystalline structure of minerals as gas that was then converted to CO_2 by a carbon electrode. The CO_2 from each sample was then analyzed by a Thermo-Finnigan DELTA^{plus}XP Isotope-Ratio Mass Spectrometer (IRMS) dual inlet (for quartz and standards) or single inlet (ore samples) with a voltage of 3 kV, 180-mm analyzer, and Universal CNOSH detector. Analytical precision based on sample duplicates was 0.4‰ and accuracy based on standards was 0.12‰. Values were reported to the delta notation (δ) in units permil related to the international Vienna Standard Mean Ocean Water (VSMOW).

PETROGRAPHY AND GEOCHEMISTRY

CGM have orthorhombic crystallography, with sites octahedrally coordinated, and forming a solid solution with the general formula AB_2O_6. Fe^{2+} and Mn^{2+} can occupy the *A*-site, while Nb^{5+} and Ta^{5+} occupy the *B*-site. In addition, some chemical impurities such as Fe^{3+}, Sc^{3+}, Ti^{4+}, Sn^{4+}, U^{4+}, W^{6+}, and REE can also be present. The columbite end-member (Nb > Ta) varies from columbite-(Fe) (ixiolite-(Fe^{2+})) to columbite-Mn (ixiolite-(Mn^{2+})), according to Fe^{2+} and Mg^{2+} contents in the *A*-site (Černý & Ercit 1989, Neiva 1996, Abdalla *et al.* 1998).

The CGM grains from the Cachoeirinha alluvial deposit display a subhedral to euhedral prismatic habit (Fig. 3A) and are typically found in association with cassiterite and wolframite. The Cachoeirinha CGM grains have gray with brown hue in color, low birefringence, and reflectance with occasional red internal reflections. Most grains exhibit from irregular to regular internal zoning patterns, as well as micro-inclusion or exsolution, observed by backscattered scanning electronic microscope (BSE-SEM) imaging (Figs. 3B–3D). These patterns are marked by increasing Ta/Nb and Mn/Fe ratios from core to rim or in isolated Ta-rich patches.

Table 1. EPMA results of the Cachoeirinha CGM grains (cation formula on the basis of six oxygen atoms).

Spots number	1	5	6	7	8	9	10	12	13	15	17	18	19	22	24	25	27	28	29	30	31	32	35	36	37	38	40	41
Nb_2O_5 (wt%)	71.16	53.72	61.09	51.63	53.44	63.72	69.17	72.85	57.05	70.93	67.20	48.77	73.45	64.05	71.07	60.21	54.54	70.56	68.86	59.83	64.19	47.38	61.95	68.80	73.12	49.02	52.07	64.08
Ta_2O_5	3.09	22.00	16.41	24.51	23.28	10.68	3.37	2.96	19.16	4.06	6.47	26.38	2.76	9.19	4.00	13.26	22.26	3.68	5.55	14.85	9.93	24.64	12.70	7.21	5.01	22.21	21.89	7.70
TiO_2	1.44	0.27	0.58	0.42	0.68	2.47	1.83	0.35	0.60	0.66	2.38	2.97	1.63	2.96	1.79	2.50	2.42	1.48	1.54	1.75	2.18	3.74	2.72	1.90	0.68	3.77	4.52	4.62
UO_2	0.33	0.36	0.34	0.32	0.34	0.28	0.28	0.37	0.30	0.31	0.43	0.30	0.34	0.38	0.23	0.32	0.36	0.37	0.38	0.40	0.36	0.40	0.33	0.34	0.27	0.31	0.36	0.45
SnO_2	0.00	1.22	0.00	0.45	0.00	0.86	0.70	0.00	0.30	0.87	0.27	0.00	0.36	0.68	0.00	0.64	0.12	0.36	0.00	0.31	0.49	1.76	1.02	0.73	0.00	1.54	1.26	0.25
SiO_2	0.06	0.38	0.28	0.53	0.43	0.24	0.07	0.09	0.36	0.04	0.14	0.43	0.06	0.14	0.05	0.23	0.36	0.05	0.07	0.27	0.14	0.52	0.24	0.14	0.10	0.31	0.41	0.10
FeO	19.30	18.29	18.65	17.99	17.59	18.32	19.35	19.99	18.58	19.38	19.01	17.16	19.50	18.78	19.41	17.66	17.53	19.40	18.86	17.85	18.39	17.21	18.34	18.63	19.51	17.63	17.02	18.74
MnO	2.33	2.38	2.39	2.41	2.57	2.67	2.43	2.35	2.41	2.38	2.78	2.48	2.16	2.41	2.30	2.77	2.67	2.34	2.18	2.44	2.63	2.42	2.30	2.25	2.45	2.28	2.52	2.77
Al_2O_3	0.00	0.00	0.01	0.00	0.01	0.00	0.02	0.00	0.00	0.01	0.03	0.00	0.00	0.00	0.01	0.03	0.03	0.00	0.01	0.00	0.01	0.00	0.00	0.02	0.00	0.01	0.00	0.01
BaO	0.08	0.00	0.00	0.00	0.08	0.07	0.12	0.05	0.00	0.03	0.00	0.00	0.02	0.20	0.06	0.12	0.00	0.08	0.00	0.13	0.08	0.06	0.07	0.01	0.19	0.09	0.09	0.01
Cr_2O_3	0.17	0.06	0.00	0.00	0.04	0.04	0.03	0.01	0.12	0.00	0.06	0.00	0.00	0.00	0.00	0.06	0.01	0.07	0.07	0.00	0.00	0.00	0.00	0.05	0.02	0.01	0.03	0.08
V_2O_5	0.07	0.01	0.00	0.04	0.07	0.09	0.07	0.00	0.04	0.04	0.08	0.08	0.10	0.03	0.00	0.03	0.00	0.05	0.04	0.06	0.00	0.12	0.04	0.06	0.08	0.12	0.06	0.12
WO_3	0.67	0.40	0.20	0.71	0.49	1.18	0.57	0.53	1.11	0.67	0.85	0.87	0.39	1.08	0.68	1.70	0.65	0.39	0.93	1.32	1.16	0.61	0.86	1.08	0.45	1.82	1.23	2.26
Total	98.71	99.10	99.96	99.01	99.03	100.61	98.01	99.55	100.03	99.38	99.70	99.44	100.77	99.90	99.59	99.51	100.94	98.83	98.48	99.20	99.54	98.85	100.57	101.21	101.88	99.11	101.46	101.18
Cation formula based on six atoms of oxygen																												
Fe (apfu)	0.931	0.959	0.939	0.951	0.922	0.893	0.943	0.961	0.950	0.938	0.919	0.899	0.919	0.917	0.930	0.881	0.889	0.938	0.921	0.901	0.905	0.902	0.900	0.890	0.920	0.917	0.854	0.893
Mn	0.114	0.127	0.122	0.129	0.137	0.132	0.120	0.114	0.125	0.117	0.136	0.131	0.103	0.119	0.112	0.140	0.137	0.115	0.108	0.125	0.131	0.129	0.114	0.109	0.117	0.120	0.128	0.134
Al	0.000	0.000	0.001	0.000	0.001	0.000	0.001	0.000	0.000	0.001	0.002	0.000	0.000	0.000	0.001	0.002	0.002	0.000	0.000	0.000	0.000	0.000	0.000	0.001	0.000	0.001	0.000	0.001
Ba	0.002	0.000	0.000	0.000	0.002	0.002	0.003	0.001	0.000	0.001	0.000	0.000	0.000	0.005	0.001	0.003	0.000	0.002	0.002	0.003	0.002	0.001	0.002	0.000	0.004	0.002	0.002	0.000
A-site total	**1.047**	**1.086**	**1.062**	**1.070**	**1.060**	**1.025**	**1.067**	**1.076**	**1.075**	**1.067**	**1.067**	**1.030**	**1.022**	**1.031**	**1.044**	**1.026**	**1.028**	**1.055**	**1.029**	**1.029**	**1.038**	**1.032**	**1.016**	**1.000**	**1.041**	**1.040**	**0.982**	**1.028**
Nb (apfu)	1.857	1.523	1.664	1.476	1.514	1.678	1.822	1.893	1.577	1.856	1.756	1.381	1.871	1.690	1.842	1.624	1.496	1.845	1.818	1.631	1.708	1.343	1.644	1.776	1.865	1.378	1.412	1.651
Ta	0.049	0.375	0.269	0.421	0.397	0.169	0.053	0.046	0.319	0.064	0.102	0.449	0.042	0.146	0.062	0.215	0.367	0.058	0.088	0.244	0.159	0.420	0.203	0.112	0.077	0.376	0.357	0.119
Ti	0.063	0.013	0.026	0.020	0.032	0.108	0.080	0.015	0.027	0.029	0.104	0.140	0.069	0.130	0.077	0.112	0.110	0.064	0.068	0.079	0.096	0.176	0.120	0.082	0.029	0.176	0.204	0.198
Sn	0.000	0.031	0.000	0.011	0.000	0.020	0.016	0.000	0.007	0.020	0.006	0.000	0.008	0.016	0.000	0.015	0.003	0.008	0.000	0.007	0.011	0.044	0.024	0.017	0.000	0.038	0.030	0.006
Si	0.004	0.024	0.017	0.033	0.027	0.014	0.004	0.005	0.022	0.002	0.008	0.027	0.003	0.008	0.003	0.014	0.022	0.003	0.004	0.016	0.008	0.033	0.014	0.008	0.006	0.019	0.025	0.006
W	0.010	0.007	0.003	0.012	0.008	0.018	0.009	0.008	0.018	0.010	0.013	0.014	0.006	0.016	0.010	0.026	0.010	0.006	0.014	0.021	0.018	0.010	0.013	0.016	0.007	0.029	0.019	0.033
Cr	0.008	0.003	0.000	0.000	0.002	0.002	0.001	0.000	0.006	0.000	0.003	0.000	0.000	0.000	0.000	0.003	0.000	0.003	0.003	0.000	0.000	0.000	0.000	0.002	0.001	0.000	0.001	0.003
V	0.003	0.000	0.000	0.002	0.003	0.004	0.003	0.000	0.002	0.001	0.003	0.003	0.004	0.001	0.000	0.001	0.000	0.002	0.002	0.003	0.000	0.005	0.001	0.002	0.003	0.005	0.002	0.005
U	0.004	0.005	0.005	0.005	0.005	0.004	0.004	0.005	0.004	0.004	0.005	0.004	0.004	0.005	0.003	0.004	0.005	0.005	0.005	0.005	0.005	0.006	0.004	0.004	0.003	0.004	0.005	0.006
B-site total	**1.998**	**1.981**	**1.984**	**1.980**	**1.988**	**2.017**	**1.992**	**1.972**	**1.982**	**1.986**	**2.000**	**2.018**	**2.007**	**2.012**	**1.997**	**2.014**	**2.013**	**1.994**	**2.002**	**2.006**	**2.005**	**2.037**	**2.023**	**2.019**	**1.991**	**2.026**	**2.056**	**2.026**
A+B total	**3.045**	**3.067**	**3.046**	**3.060**	**3.048**	**3.042**	**3.059**	**3.048**	**3.057**	**3.043**	**3.067**	**3.048**	**3.029**	**3.043**	**3.041**	**3.040**	**3.041**	**3.049**	**3.031**	**3.035**	**3.043**	**3.069**	**3.039**	**3.019**	**3.032**	**3.066**	**3.038**	**3.054**
Mn/(Mn+Fe)	0.109	0.117	0.115	0.119	0.129	0.129	0.113	0.106	0.116	0.111	0.129	0.128	0.101	0.115	0.107	0.137	0.133	0.109	0.105	0.122	0.126	0.125	0.109	0.109	0.113	0.116	0.130	0.130
Ta/(Nb+Ta)	0.025	0.198	0.139	0.222	0.208	0.092	0.028	0.024	0.168	0.033	0.055	0.245	0.022	0.079	0.033	0.117	0.197	0.030	0.046	0.130	0.085	0.238	0.025	0.059	0.040	0.214	0.202	0.067

Table 1. Continuation.

| Spots number	42	43	44	45	46	47	48	49	50	51	52	54	55	56	58	59	60	61	62	63	65	66	67	69	70	73	76
Nb₂O₅ (wt%)	57.87	54.09	67.47	47.84	68.87	47.97	58.84	71.73	64.61	47.23	60.18	47.63	50.99	72.31	53.80	60.23	45.98	70.94	72.74	48.78	62.61	53.50	46.37	66.23	58.80	58.95	69.19
Ta₂O₅	15.69	19.72	6.97	26.73	7.41	26.69	16.64	3.09	10.56	30.33	14.64	30.83	24.96	3.54	22.80	10.38	29.44	4.80	4.00	23.77	13.85	25.16	31.43	9.34	15.66	13.03	6.08
TiO₂	3.54	3.49	1.63	2.65	2.27	3.05	2.69	1.53	2.13	2.15	2.16	1.34	2.12	2.03	2.40	4.07	2.74	2.10	2.11	2.36	0.44	0.62	0.63	2.03	1.08	2.95	2.02
UO₂	0.42	0.38	0.38	0.31	0.34	0.34	0.41	0.33	0.38	0.38	0.45	0.41	0.38	0.31	0.35	0.35	0.39	0.32	0.39	0.42	0.39	0.35	0.26	0.37	0.45	1.57	0.33
SnO₂	1.01	0.00	0.00	0.00	0.11	0.00	0.30	0.00	0.00	0.20	0.00	0.87	0.00	0.52	0.62	0.67	1.11	0.00	0.00	1.34	0.00	0.82	0.00	0.70	0.33	0.23	0.65
SiO₂	0.27	0.32	0.07	0.50	0.08	0.44	0.31	0.04	0.15	0.59	0.21	0.62	0.48	0.09	0.44	0.21	0.56	0.09	0.03	0.37	0.23	0.39	0.56	0.20	0.35	0.29	0.10
FeO	18.33	17.93	19.28	17.29	18.85	17.43	18.15	19.50	18.52	17.00	18.42	17.33	17.39	19.67	17.60	18.06	17.05	19.29	19.54	17.93	18.81	18.24	17.86	18.77	18.73	12.01	11.63
MnO	2.73	2.92	2.40	2.50	2.43	2.33	2.34	2.46	2.58	2.58	3.16	2.16	2.92	2.31	2.51	2.83	2.64	2.31	2.30	2.63	2.67	2.14	2.18	2.57	1.93	8.10	9.74
Al₂O₃	0.02	0.00	0.01	0.00	0.01	0.00	0.00	0.01	0.01	0.00	0.01	0.00	0.02	0.00	0.00	0.00	0.00	0.01	0.00	0.00	0.00	0.00	0.00	0.00	0.00	0.01	0.00
BaO	0.07	0.08	0.16	0.00	0.16	0.17	0.11	0.10	0.00	0.12	0.07	0.03	0.00	0.03	0.03	0.04	0.18	0.08	0.01	0.16	0.03	0.05	0.00	0.00	0.00	0.00	0.00
Cr₂O₃	0.00	0.00	0.00	0.00	0.06	0.06	0.08	0.00	0.13	0.02	0.02	0.00	0.00	0.10	0.08	0.03	0.02	0.00	0.06	0.05	0.02	0.12	0.00	0.00	0.00	0.09	0.01
V₂O₅	0.06	0.11	0.00	0.05	0.01	0.06	0.08	0.00	0.05	0.07	0.09	0.04	0.11	0.07	0.04	0.08	0.11	0.02	0.08	0.01	0.00	0.00	0.05	0.07	0.11	0.04	0.00
WO₃	1.52	1.55	1.17	0.84	0.64	0.73	1.38	0.57	1.00	0.70	1.29	0.33	0.78	0.77	0.93	2.37	0.67	1.08	0.50	1.44	0.45	0.28	0.33	1.20	0.93	1.24	1.98
Total	101.50	100.59	99.53	98.72	101.25	99.26	101.32	99.36	100.11	101.36	100.70	101.59	100.13	101.72	101.61	99.33	100.89	101.04	101.76	99.26	99.50	101.67	99.67	101.47	98.37	98.50	101.73
Cation formula based on six atoms of oxygen																											
Fe (apfu)	0.902	0.904	0.940	0.917	0.899	0.917	0.898	0.936	0.906	0.890	0.914	0.910	0.902	0.921	0.890	0.889	0.895	0.914	0.914	0.944	0.945	0.938	0.963	0.903	0.958	0.606	0.552
Mn	0.136	0.149	0.119	0.134	0.117	0.124	0.117	0.120	0.128	0.137	0.159	0.115	0.153	0.109	0.129	0.141	0.140	0.111	0.109	0.140	0.136	0.112	0.119	0.125	0.100	0.414	0.468
Al	0.001	0.000	0.000	0.000	0.001	0.000	0.000	0.001	0.001	0.000	0.001	0.000	0.001	0.000	0.000	0.000	0.000	0.001	0.000	0.000	0.000	0.000	0.000	0.000	0.000	0.001	0.000
Ba	0.002	0.002	0.004	0.000	0.004	0.004	0.003	0.002	0.000	0.003	0.002	0.001	0.000	0.001	0.001	0.001	0.004	0.002	0.000	0.004	0.001	0.001	0.000	0.000	0.000	0.000	0.000
A-site total	**1.041**	**1.053**	**1.063**	**1.050**	**1.021**	**1.045**	**1.018**	**1.059**	**1.035**	**1.030**	**1.076**	**1.026**	**1.056**	**1.031**	**1.020**	**1.031**	**1.039**	**1.028**	**1.023**	**1.088**	**1.082**	**1.051**	**1.082**	**1.028**	**1.058**	**1.001**	**1.020**
Nb (apfu)	1.541	1.475	1.779	1.370	1.776	1.365	1.574	1.860	1.709	1.336	1.614	1.352	1.430	1.831	1.471	1.603	1.305	1.816	1.840	1.388	1.701	1.488	1.351	1.723	1.626	1.608	1.774
Ta	0.251	0.323	0.110	0.461	0.115	0.457	0.268	0.048	0.168	0.516	0.236	0.526	0.421	0.054	0.375	0.166	0.503	0.074	0.061	0.407	0.226	0.421	0.551	0.146	0.260	0.214	0.094
Ti	0.157	0.158	0.071	0.126	0.097	0.145	0.120	0.066	0.094	0.101	0.096	0.063	0.099	0.085	0.109	0.180	0.129	0.089	0.089	0.112	0.020	0.029	0.031	0.088	0.050	0.134	0.086
Sn	0.024	0.000	0.000	0.000	0.002	0.000	0.007	0.000	0.000	0.005	0.000	0.022	0.000	0.012	0.015	0.016	0.028	0.000	0.000	0.034	0.000	0.020	0.000	0.016	0.008	0.005	0.015
Si	0.016	0.019	0.004	0.031	0.005	0.028	0.018	0.002	0.009	0.037	0.012	0.039	0.029	0.005	0.026	0.012	0.035	0.005	0.002	0.023	0.014	0.024	0.036	0.012	0.022	0.018	0.006
W	0.023	0.024	0.018	0.014	0.010	0.012	0.021	0.008	0.015	0.011	0.020	0.005	0.012	0.011	0.015	0.036	0.011	0.016	0.007	0.023	0.007	0.004	0.005	0.018	0.015	0.019	0.029
Cr	0.000	0.000	0.000	0.000	0.003	0.003	0.004	0.000	0.006	0.001	0.001	0.000	0.000	0.004	0.004	0.002	0.001	0.000	0.003	0.002	0.001	0.006	0.000	0.000	0.000	0.004	0.001
V	0.002	0.004	0.000	0.002	0.001	0.002	0.003	0.000	0.002	0.003	0.003	0.001	0.004	0.002	0.002	0.003	0.005	0.001	0.003	0.000	0.000	0.000	0.002	0.003	0.004	0.002	0.000
U	0.005	0.005	0.005	0.004	0.004	0.005	0.005	0.004	0.005	0.003	0.006	0.006	0.005	0.002	0.005	0.005	0.006	0.004	0.005	0.006	0.005	0.005	0.004	0.005	0.006	0.021	0.004
B-site total	**2.027**	**2.010**	**1.987**	**2.009**	**2.003**	**2.016**	**2.020**	**1.989**	**2.006**	**2.016**	**1.988**	**2.008**	**2.000**	**2.008**	**2.022**	**2.024**	**2.023**	**2.005**	**2.010**	**1.996**	**1.974**	**1.997**	**1.980**	**2.009**	**1.991**	**2.045**	**2.008**
A+B total	**3.068**	**3.063**	**3.050**	**3.059**	**3.024**	**3.061**	**3.038**	**3.048**	**3.041**	**3.046**	**3.064**	**3.040**	**3.056**	**3.039**	**3.042**	**3.055**	**3.062**	**3.033**	**3.033**	**3.084**	**3.056**	**3.048**	**3.062**	**3.037**	**3.049**	**3.046**	**3.028**
Mn/(Mn+Fe)	0.131	0.142	0.112	0.128	0.116	0.119	0.115	0.113	0.124	0.133	0.148	0.112	0.145	0.106	0.126	0.137	0.136	0.108	0.107	0.129	0.126	0.106	0.110	0.122	0.094	0.406	0.459
Ta/(Nb+Ta)	0.140	0.180	0.058	0.252	0.061	0.251	0.145	0.025	0.089	0.279	0.128	0.280	0.227	0.029	0.203	0.094	0.278	0.039	0.032	0.227	0.117	0.220	0.290	0.078	0.138	0.117	0.050
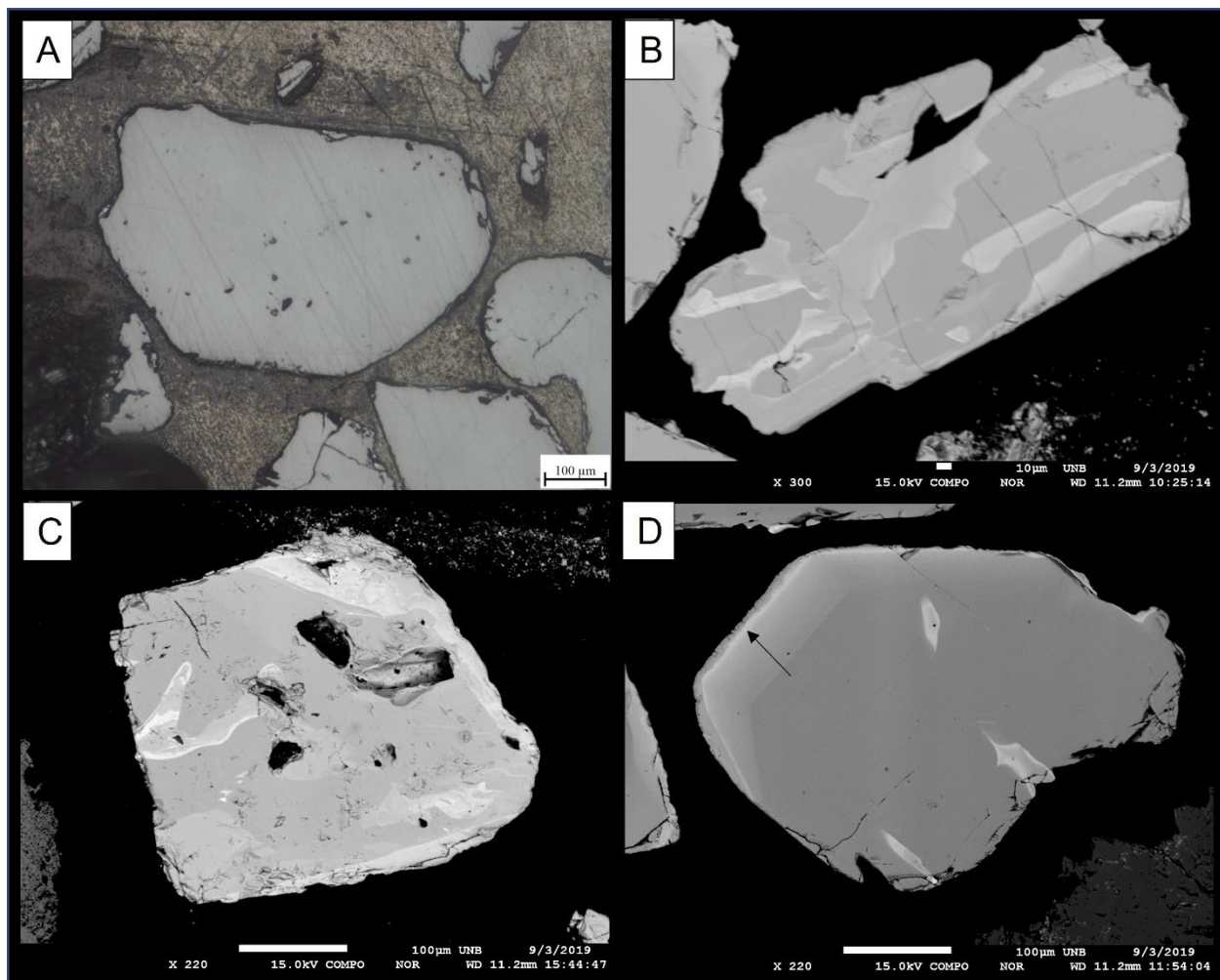
Figure 3. Petrographic images of CGM grains of the Cachoeirinha alluvial deposit. (A) Plane-polarized photomicrography by reflected lights. (B–D) SEM images of CGM grains with irregular and normal zoning (images obtained from combined BSE and secondary electrons).

EPMA confirmed the initial SEM qualitative analyses, indicating that the Ta content varies according to the internal zoning pattern in CGM grains (Table 1): lighter areas observed by BSE imaging hold higher Ta concentrations (Figs. 4A and 4B). Normally, CGM grains with a regular or normal zoning have Ta contents increase from core to rim. In contrast, CGM grains with irregular or heterogeneous zoning do not display a continuous rise in Ta or Nb contents. This chemical variation has been expected because Ta_2O_5 and Nb_2O_5 contents in CGM are inversely proportional (Figs. 4C and 4D). However, some crystals have different zoning styles (e.g., discontinuous, curved, and oscillatory) along the boundaries between Ta-rich and Nb-rich phases. This suggests that there is some reabsorption of columbite by a posterior Ta-rich phase or even Ta-rich nuclei within a homogeneous Nb-rich crystal (e.g., Tindle & Breaks 2000, Chevychelov et al. 2010, Neiva et al. 2015).

Unlike the inverse correlation observed between Nb and Ta contents in CGM grains, the Sn and Ti contents show a tendency toward a direct proportional correlation (Figs. 4E and 4F). These chemical data suggest the occurrence of coupled ionic substitutions into the octahedral A- and B-sites, involving Fe and Mn, according to the following equation: $3(Sn, Ti)^{4+} \leftrightarrow 2(Nb, Ta)^{5+} + (Fe, Mn)^{2+}$. These substitutions favor the

zoning and chemical variation in the CGM grains (Möller et al. 1988, Černý & Ercit 1989, Neiva 2008, Neiva et al. 2015). These substitutions can also be observed by a negative pattern of apfu correlation diagrams between Nb vs Ta, Sn+Ti vs Nb+Ta, and Sn+Ti vs Fe+Mn+Nb+Ta (Figs. 5A–5C). On the contrary, the variable contents identified for Si, Al, Ba, Cr, V, W, REE, and U (Table 2) reveal the occurrence of other complex types of coupled ionic substitution mechanisms during the nucleation and mineral growth, which also occurred into the octahedral A- and B-sites. These mechanisms can be represented by the following general equation: $3(Sn, Ti, U, Si)^{4+} + (W, Cr)^{6+} \leftrightarrow 2(V, Nb, Ta)^{5+} + 2(Al, REE)^{3+} + (Fe, Mn, Ba)^{2+}$ (adapted from Wenger et al. 1991, Wise et al. 1998, Neiva et al. 2015). Despite the apparent complexity of coupled ionic substitutions, the main mechanism involves substitutions of an octahedral single site (B-site = Nb $\leftrightarrow$ Ta).

In the (Sn,Ti,W)-(Nb,Ta)-(Fe,Mn) triangular diagram, the Cachoeirinha CGM grains plot in clusters between columbite-ixiolite fields distributed along the alignment (Sn,Ti,W)-$(Fe,Mn)(Nb,Ta)_2$ join (Fig. 5D). This chemical feature suggests that Sn+Ti are mainly partitioned into the B-site, favoring the generation of a molecular mineral phase named pseudo-ixiolite $((Ta, Nb, Sn, Ti, Fe, Mn)_4O_8)$, probably associated with
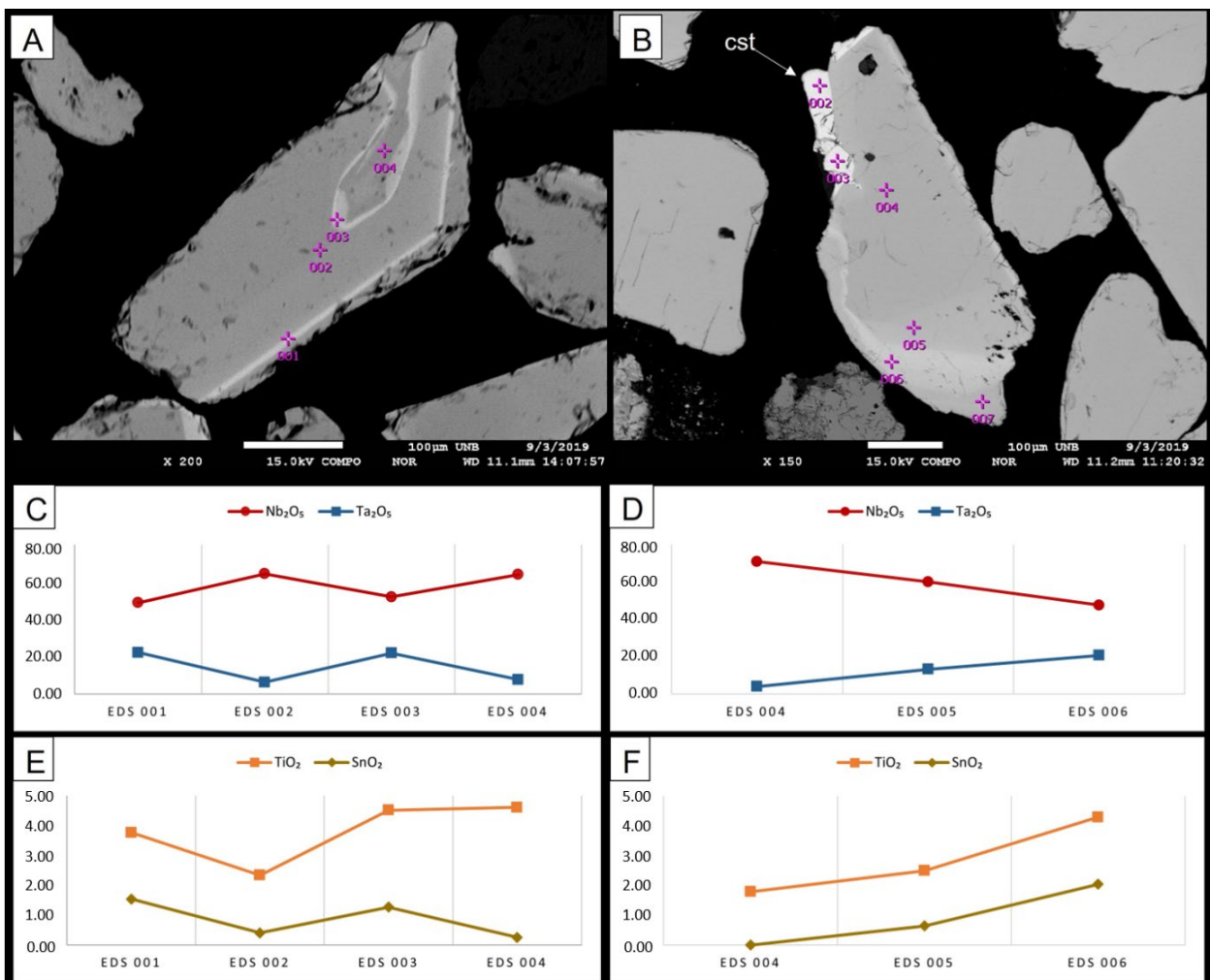
Figure 4. EPMA analyzed spots on the Cachoeirinha CGM grains. (A and B) SEM images of CGM grains with spots location. (C–F) Profiles showing the respective variation of Nb_2O_5, Ta_2O_5, TiO_2, and SnO_2 contents.

some degree of disordered in the CGM crystalline structure at higher temperatures (Tindle & Breaks 2000, Bartels *et al.* 2010, Wise & Brown 2011, Badanina *et al.* 2015). On the quadrilateral compositional diagram, the EPMA data plot mostly in the columbite-(Fe) field, but there are a few rare data points plotted close to the intermediate field (Fig. 5E). The vertical trend observed is the result of the orientation EPMA spots from core to rim of the columbite-(Fe) grains. This orientation generated different Ta/(Nb+Ta) ratios, which are a response to internal zoning diagnosed by BSE-SEM imaging. On the contrary, some individual grains show the central portion enriched in Nb and rims enriched in Ta. In general, the EPMA data pointed to columbite-(Fe) as the dominant phase, represented by the (apfu)-general formula: $A(Fe_{0.552-0.979} - Mn_{0.095-0.414}) B(Ta_{0.042-0.551} - Nb_{1.305-1.871})_2O_6$, with ionic impurities mainly in the octahedral *B*-site.

The LA-ICP-MS analysis on the Cachoeirinha CGM grains revealed a high total REE content (Table 2). In general, the chondrite-normalized REE patterns show that ΣREE_N is above 1, indicating depleted light rare earth elements ($LREE_N$), with strong negative Eu anomalies ($Eu/Eu^* = 0.02-0.15$), and enriched heavy rare earth element ($HREE_N$) patterns (Fig. 6). The $LRRE_N$ patterns are variable, but most samples have a positive anomaly in Ce. Heavy REE_N (Er, Tm, Yb, Lu) predominate over middle REE_N (Gd, Tb, Dy, Ho), with (Gd/Lu)$_N$ ratios = 0.01–0.04. However, it is possible to observe two groups of samples (CGM1 and CGM2) that differ mainly in relation to $MREE_N$ and $HREE_N$, suggesting different generations of Cachoeirinha CGM grains. CGM1 have $MREE_N$ = 2067–6543, $HREE_N$ = 24369–67016, with (HREE/MREE)$_N$ ≥ 10, while CGM2 have $MREE_N$ = 506–640, $HREE_N$ = 3200–6400, with (HREE/MREE)$_N$ ≤ 10. According to Graupner *et al.* (2010), modification of the (HREE/MREE)$_N$ ratios can indicate an increasing degree of fractionation.

In addition, the wide UO_2 content, from 0.01 to 2.38 wt.% in Cachoeirinha CGM grains, allowed us to perform in situ U-Pb isotopic dating by LA-ICP-MS, following the method presented by Che *et al.* (2015) and Legros *et al.* (2019).

OXYGEN ISOTOPE

Oxygen isotopic ($\delta^{18}O$) data have been widely used to characterize the nature of fluids and geothermometric conditions during ore formation (Alderton 1989, Zheng 1991, Zhang *et al.* 1994, Moon *et al.* 1996, Chen *et al.* 2018, Vho *et al.* 2019). Oxygen isotopic analyses on the Cachoeirinha CGM grains
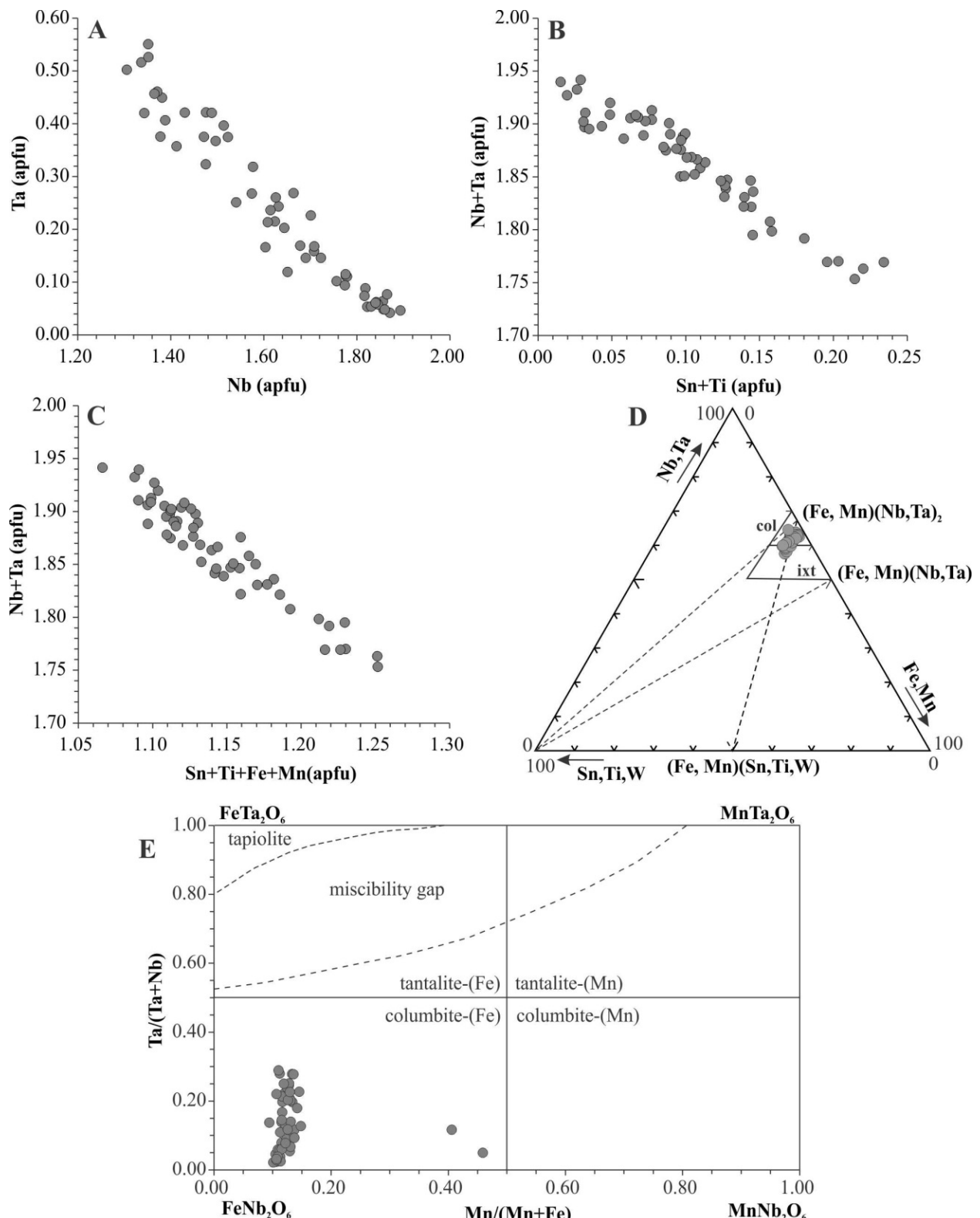
Figure 5. Chemical correlation diagrams applied to the Cachoeirinha CGM grains. (A) Nb vs Ta apfu diagram with a negative correlation. (B and C) Sn+Ti vs Nb+Ta and Sn+Ti vs Fe+Mn+Nb+Ta apfu diagrams also with negative proportional correlation. (D) (Sn,W,Ti)-(Fe,Mn)-(Nb,Ta) triangular diagram with samples plots between columbite-ixiolite fields (adapted from Neiva *et al.* 2015). (E) Composition diagram indicating the dominant presence of columbite-(Fe). A steep vertical trend is noticeable with Ta/(Nb+Ta) varying from 0.02 to 0.41 (immiscibility gap as defined by Černý and Ercit 1989).

revealed $\delta^{18}O = 2.78‰$ value. These isotopic data are consistent with available data on cassiterite ($\delta^{18}O = 1.6–3.3‰$) and wolframite ($\delta^{18}O = 0.6–1.6‰$) associated with the evolved/fractionated hydrothermal-magmatic system from the Rondônia Intrusive Suite (*e.g.*, Souza & Botelho 2009, Nascimento &

Souza 2017). Normally, cassiterite, wolframite, and columbite-tantalite linked to hydrothermal-magmatic system show $\delta^{18}O < 5‰$ due to their greater susceptibility to isotopic fractionation during temperature drop (Zhang *et al.* 1994, Li *et al.* 2022). However, the chemical variations, zoning, intergrowth,

Table 2. REE content obtained by the LA-ICP-MS analysis using polished section of the Cachoeirinha CGM grains.

Types	CGM1						CGM2		
Spots	1	2	4	6	7	9	3	5	8
^{139}La (ppm)	285	203	6	3.6	14	14	16	7	1.4
^{140}Ce	256	1323	13	104	39	375	21	110	36
^{141}Pr	34	16	3.6	4.3	5.1	5.6	2.5	1.05	0.28
^{146}Nd	59	113	26	24	23	63	10	5.2	2.1
^{147}Sm	10	41	26	36	21	29	3.4	9	3.2
^{153}Eu	0.29	2.4	1.14	0.56	0.41	0.31	0.02	0.35	0.06
^{157}Gd	20	58	45	62	39	61	5.8	10	6.3
^{159}Tb	10	41	25	28	21	45	3.3	4.4	4.1
^{163}Dy	161	400	343	417	332	519	37	34	54
^{165}Ho	56	155	108	161	132	158	15	11	15
^{166}Er	341	853	642	898	664	984	91	49	67
^{169}Tm	112	257	236	259	193	327	27	12	30
^{172}Yb	1,253	3,272	3,008	3,317	2,454	3,563	269	170	385
^{175}Lu	244	741	504	745	549	629	56	35	59
Eu/Eu*	0.06	0.15	0.10	0.04	0.04	0.02	0.01	0.11	0.04
(Gd/Lu)$_N$	0.01	0.01	0.01	0.01	0.04	0.01	0.01	0.01	0.01
MREE$_N$	2,067	5,904	4,294	5,734	4,557	6,543	550	506	640
HREE$_N$	24,369	66,201	52,749	67,016	49,155	67,074	5,632	3,275	6,417
(HRRE/MREE)$_N$	11.78	11.21	12.28	11.68	10.78	10.25	10.23	6.47	10.01
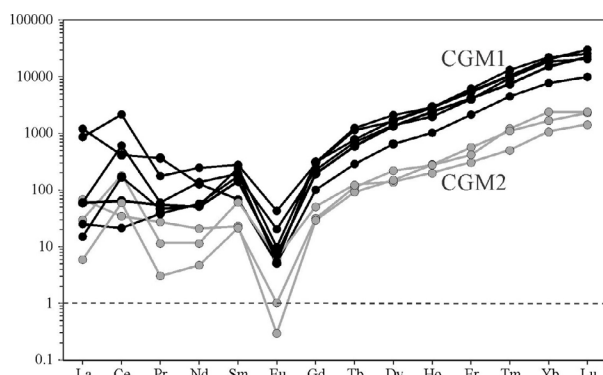
Figure 6. Chondrite-normalized REE patterns of the Cachoeirinha CGM grains (after McDonough & Sun 1995). Note the two sets of samples with different MREEN and HREEN contents.

and micro-inclusions commonly found in these ore minerals may also interfere, to some degree, with the accuracy of oxygen isotopic measurements.

U-Pb GEOCHRONOLOGY

The U-Pb geochronology data are presented in Table 3, and the results are discussed below. In general, on back-scattered electron (BSE) images, the Cachoeirinha CGM grains analyzed have subhedral to euhedral prismatic shapes, with lengths exceeding 1 mm. These grains also display slight internal zoning and minimal fracturing (Fig. 7A).

The U-Pb data produced two different age sets (Fig. 7B). The older component showed a lower intercept of 1059 ± 10 Ma on a Tera Wasserburg diagram. However, within uncertainty of the

same data on a concordia diagram if 5 of the 11 spots that have higher common Pb are excluded, resulting in an age of 1052 ± 6 Ma (Fig. 7C). The younger component, composed by mostly subconcordant to discordant data, yielded a lower intercept age of 909 ± 7 Ma on a Tera Wasserburg diagram (Fig. 7D).

In general, depleted U (ca. 100–250 ppm) relative to the younger population (ca. 400–690 ppm U) marks the older age cluster. Th/U shows an opposite behavior, with typically higher values observed in older age domains (> 0.15) compared with younger ages (< 0.15), although there are a few exceptions. In addition, the older age cluster has an initial ^{207}Pb/^{206}Pb ratio $= 0.354 \pm 0.024$, while the younger population has an initial ^{207}Pb/^{206}Pb ratio $= 0.613 \pm 0.079$ (see supplement with analytical data in https://doi.org/10.17605/OSF.IO/V89YB). On the contrary, we observe that the set of Cachoeirinha CGM grains with younger ages tends to have high MREE$_N$ and HREE$_N$, therefore with some affinity to the CGM1 type. However, further complementary LA-ICP-MS analyses are still necessary to statistically prove this geochemical affinity.

DISCUSSION

The orthorhombic CGM form a solid solution between (Nb, Ta)-(Fe, Mn) end-members common in LCT (Li, Cs, Ta) and NYF (Nb, Y, F) fractionated granite-pegmatite systems, normally associated with cassiterite, wolframite, and others metallic minerals (Černý & Ercit 1989, Černý *et al.* 2005, Graupner *et al.* 2010). In these magmatic or hydrothermal-magmatic systems, physicochemical oscillations (e.g., temperature, pressure, fO_2, and pH) interfere with the degree of order-disorder in the CMG crystalline structure (Wang *et al.* 1982, Linnen

Table 3. U-Pb geochronology results of the Cachoeirinha CGM grains.

Older age group

Spots CCGM					Data for Tera-Wasserburg plot[b]						Data for Wetherill plot[c]					Dates[c]									%
age group	f206c	^{206}Pb (cps)	U (µg g^{-1})[a]	Th/U	^{206}Pb/^{204}Pb	1s (%)	^{238}U/^{206}Pb	1s (%)	^{207}Pb/^{206}Pb	1s (%)	^{207}Pb/^{235}U	1s (%)	^{206}Pb/^{238}U	1s (%)	Rho	^{207}Pb/^{206}Pb	2s abs	2s sys abs	^{206}Pb/^{238}U	2s abs	2s sys abs	^{207}Pb/^{235}U	2s abs	2s sys abs	conc[d]
9	5.79	239,391	235	0.34	-244	-89.7	4.88	1.7	0.11883	2.94	3.4917	2.8	0.20647	1.5	0.00	1919	110	110	1,216	35	35	1,508	43	44	63.3
11	0.62	162,868	202	0.26	-2,627	-6.48	5.66	0.9	0.07256	1.37	1.7947	1.1	0.17811	0.9	0.15	972	53	53	1,056	17	17	1,039	14	14	108.6
12	0.50	267,461	335	0.06	-3,754	-8.72	5.65	0.8	0.07270	1.29	1.7933	1.2	0.17811	1.0	0.59	992	44	44	1,055	20	20	1,038	15	15	106.4
13	0.29	198,987	251	0.12	-3,784	-6.53	5.69	1.1	0.07460	1.73	1.8234	1.6	0.17854	1.1	0.30	1003	66	66	1,058	22	22	1,047	19	19	105.4
14	0.32	171,217	222	0.16	-3,004	-6.25	5.65	1.0	0.07440	1.94	1.8258	1.6	0.17894	0.9	0.09	962	54	54	1,060	18	18	1,046	18	19	110.1
15	0.10	207,121	262	0.30	-3,517	-5.37	5.67	0.9	0.07359	2.09	1.8308	2.1	0.17828	0.9	0.08	955	48	48	1,057	17	17	1,036	17	17	110.7
16	9.48	123,363	102	0.36	8.3	764	3.83	1.0	0.16224	1.52	5.9354	1.3	0.26383	1.0	0.05	2462	46	46	1,508	27	27	1,959	21	22	61.2
17	0.65	113,639	144	0.16	-1,689	-6.03	5.69	1.2	0.07478	2.17	1.8319	2.3	0.17576	1.3	0.13	986	71	71	1,042	25	25	1,040	21	21	105.6
18	0.83	161,442	187	0.18	-1,965	-10.0	5.54	1.5	0.08024	1.97	2.0196	2.0	0.18281	1.4	0.30	1166	73	73	1,081	27	27	1,113	25	25	92.7
19	3.20	150,327	169	0.25	-695	-16.7	5.16	1.1	0.09842	2.09	2.7179	2.5	0.19728	1.1	0.32	1509	72	72	1,159	23	23	1,308	32	33	76.8
20	2.19	159,255	190	0.19	-1,082	-13.2	5.42	0.9	0.08594	1.87	2.2251	1.7	0.18621	0.9	0.00	1279	67	67	1,100	19	19	1,178	22	23	86.0

Younger age group

Spots CCGM					Data for Tera-Wasserburg plot[b]						Data for Wetherill plot[c]					Dates[c]									%
age group	f206c	^{206}Pb (cps)	U (ppm)	Th/U	^{206}Pb/^{204}Pb	1s (%)	^{238}U/^{206}Pb	1s (%)	^{207}Pb/^{206}Pb	1s (%)	^{207}Pb/^{235}U	1s (%)	^{206}Pb/^{238}U	1s (%)	Rho	^{207}Pb/^{206}Pb	2s abs	2s sys abs	^{206}Pb/^{238}U	2s abs	2s sys abs	^{207}Pb/^{235}U	2s abs	2s sys abs	conc[d]
1	1.33	340,612	485	0.11	-3,339	-11.9	6.58	0.6	0.08103	1.08	1.7386	1.0	0.15327	0.6	1,202	39	39	919	11	11	1,019	12	12	1,202	76.5
2	15.08	198,719	207	0.30	162	6.5	5.19	1.2	0.18150	1.78	4.9409	1.7	0.19387	1.2	2,658	54	54	1141	25	25	1,801	28	28	2,658	42.9
3	0.60	315,921	428	0.09	-6,451	-6.0	6.56	0.8	0.07292	1.50	1.5457	1.2	0.15348	0.8	960	55	55	920	13	13	945	14	15	960	95.8
4'	0.68	399,123	587	0.09	-5,705	-9.2	6.84	0.8	0.07457	1.29	1.5217	1.1	0.14698	0.8	1,022	51	51	883	13	13	936	13	14	1,022	86.4
5	0.26	309,216	411	0.09	-6,287	-7.0	6.48	0.9	0.07299	1.54	1.5714	1.4	0.15526	0.9	999	69	69	930	16	16	955	16	17	999	93.0
6	1.00	278,358	407	0.21	-3,409	-14.9	6.48	0.8	0.07594	1.43	1.6295	1.4	0.15461	0.9	1,072	55	55	929	15	15	979	17	17	1,072	86.7
7	1.25	320,941	441	0.33	-2,503	-14.4	6.51	0.7	0.08323	1.53	1.8292	1.9	0.15477	0.7	1,222	46	46	927	12	12	1,034	14	15	1,222	75.8
8	0.61	480,505	693	0.12	-5,318	-13.6	6.54	0.9	0.07571	1.37	1.6242	1.2	0.15431	0.9	1,060	53	53	925	15	15	977	14	14	1,060	87.2
10	0.25	301,173	442	0.14	-5,403	-8.7	6.52	1.0	0.07475	1.84	1.5803	1.6	0.15348	1.1	1,038	74	74	920	18	18	959	19	19	1,038	88.6

[a]Concentration uncertainty ca. 20%; [b]data not corrected for common-Pb; [c]data corrected/not corrected for common-Pb; [d]concordance calculated as (^{206}Pb-^{238}U age/^{207}Pb-^{206}Pb age)*100; *unused data; Decay constants of Jaffey *et al.* (1971) used; Total systematic uncertainties (ssys): ^{206}Pb/^{238}U = 1.0%, ^{207}Pb/^{206}Pb = 0.55% (2 s). bd = below detection; #N/A = not available; Uncertainties quoted without components related to systematic error unless otherwise stated;
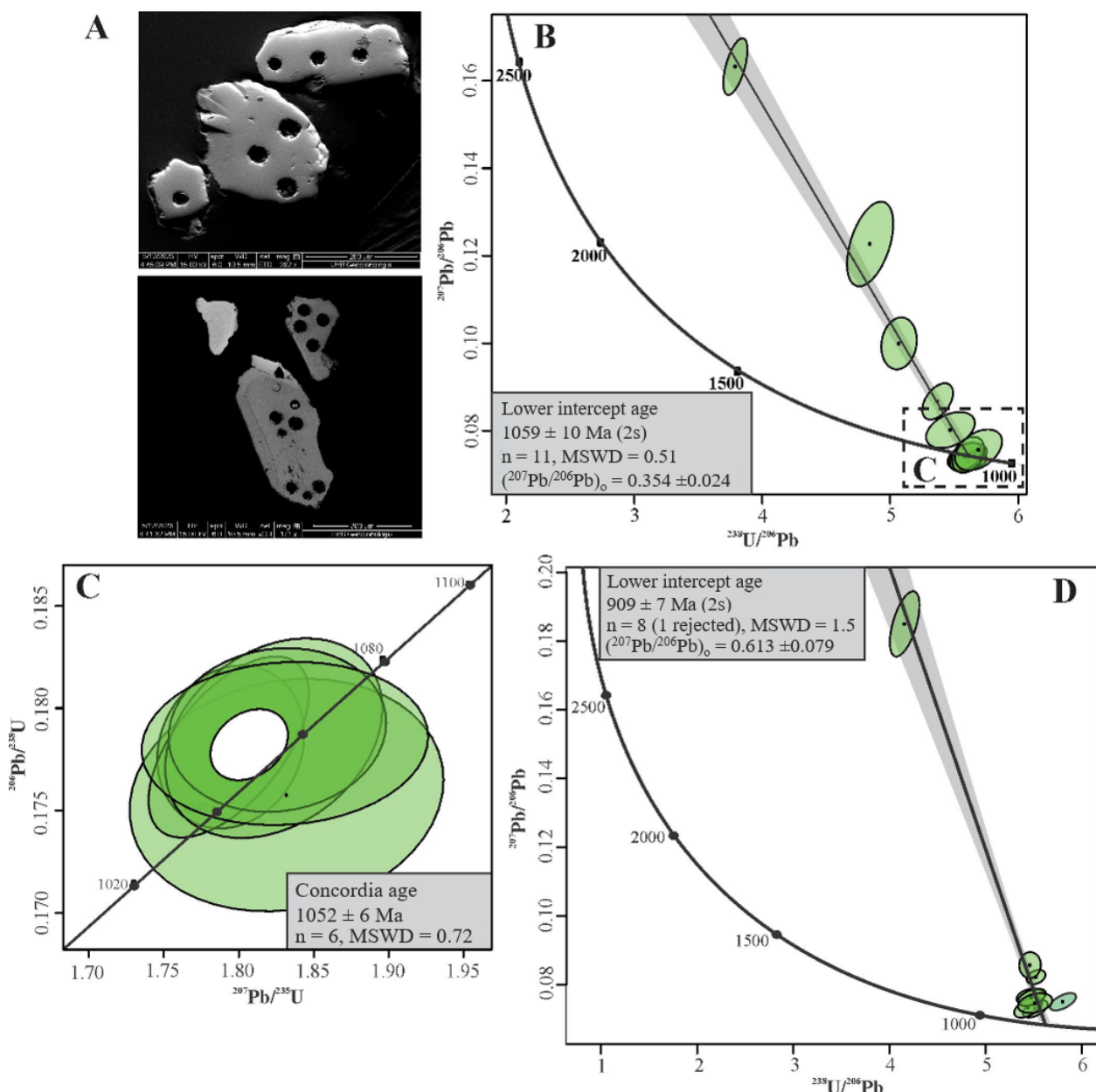
Figure 7. (A) Backscattered electron images of the Cachoeirinha CGM grains showing spots analyzed for U-Pb geochronology. (B) Tera-Wasserburg diagram. Free regression to a lower intercept age of older domains. (C) Selection of the most concordant and common-Pb free spots to produce a concordia age of 1052 ± 6 Ma. (D) The lower intercept younger age obtained from the same samples is 909 ± 7 Ma.

& Keppler 1997, Lichtervelde *et al.* 2007, Wise *et al.* 2012). This process can favor Nb/Ta and Fe/Mn substitution, as well as the entry of certain chemical impurities (Sn, Ti, W, U, and others) through coupled substitutions when the temperature drops within deposition sites (Černý *et al.* 1986, Hannah & Stein 1990, Uher *et al.* 1998, Černý & Ercit 1989, Wise *et al.* 2012, Neiva *et al.* 2015). As a result, CGM ± (cassiterite and wolframite) typically exhibit chemical variations, zoning, and mineral intergrowth (Raimbault *et al.* 1995, Breiter *et al.* 2017, González *et al.* 2017, Wu *et al.* 2020, Yin *et al.* 2020).

The chemical variations and internal zoning observed in the Cachoeirinha CGM are the results of variation in the Ta/(Nb+Ta) ratio from the core to the rim of the grains. These are common characteristics also observed in other CGM occurrences worldwide (*e.g.,* Tindle & Breaks 2000, Anderson *et al.* 2013, Melcher *et al.* 2015, Siachoque *et al.* 2020). However,

the mechanisms proposed to explain the chemical variation and the different zoning types in CGM are still debatable. In general, various mechanisms of simultaneous and/or cyclic substitution have been proposed, including (a) fluctuation in the Nb/Ta ratio during the hydrothermal-magmatic phase, leading to resorption mechanisms from the rim to the core of primary mineral grains; (b) substitution or partial reabsorption of columbite by a Ta-rich later phase during the final stages of crystallization; (c) cyclic interactions between melt and fluids during crystal growth and temperature reduction; and (d) Ta exsolution during a rapid temperature drop, due to tantalum's affinity for lower temperatures during crystallization (Wang *et al.* 1982, Černý *et al.* 1985, Lahti 1987, Černý and Ercit 1989, Abdalla *et al.* 1998, Neiva *et al.* 2015).

The different zoning types (regular, irregular, and isolated Ta-rich patches) identified in the Cachoeirinha CGM

grains indicate that various mineral substitution mechanisms occurred concomitantly and/or cyclically during the temperature drops. The mineral chemistry data point to columbite-(Fe) as the dominant phase, but with a wide variation in the Ta/(Ta+Nb) ratio, indicating oscillations between the (Nb, Ta) end-members from the core to the rim. The occasional Ta-rich patches may be linked to the exsolution process, while the rare variation in the Mn/(Mn+Fe) ratio identified at the core portion may be related to oscillations in the oxidation state of the hydrothermal-magmatic system or caused by CGM in different generations (Chudík *et al.* 2008, Melcher *et al.* 2017, Yin *et al.* 2020).

Under a specific range of temperature and pressure, the variation in the Mn/(Mn+Fe) ratio may allow coupled ionic substitutions that favor the entry of chemical impurities (Sn, Ti, Ta, Si, Al, Ba, Cr, V, W, REE, and U). These types of substitutions can be represented according to the following equation:

$$3(Sn, Ti, U, Si)^{4+} + (W, Cr)^{6+} \leftrightarrow 2(V, Nb, Ta)^{5+} + 2(Al, REE)^{3+} + (Fe, Mn, Ba)^{2+}$$ (adapted from Neiva *et al.* 2015, Siachoque *et al.* 2020). The EPMA chemical results point to the following (apfu)-general formula of Cachoeirinha columbite-(Fe): $(Fe_{0.552-0.979} - Mn_{0.095-0.414})(Ta_{0.042-0.551} - Nb_{1.305-1.871})_2O_6$, with ionic impurities mainly in the octahedral *B*-site. In addition, the LA-ICP-MS analysis revealed a high total REE concentration, mainly in $MREE_N$ and $HREE_N$, which would also enter as impurities in site *B*-site.

Oxygen isotope studies in cassiterite and wolframite from Rondônia Tin Province indicate significant isotopic fractionation during the rise of the hydrothermal-magmatic system. This fractionation is typically associated with the presence of mixed fluid phases ($NaCl-H_2O + NaCl-H_2O-CO_2-CH_4-N_2 + CO_2 + CO_2-CH_4$) trapped at temperatures between 480 and 300°C (Leite Jr. 2002, Souza & Botelho 2002, 2009, Souza 2003, Sparrenberger 2003, Bettencourt *et al.* 2005, Nascimento & Souza 2017). The Cachoeirinha columbite-(Fe) presents lowered $\delta^{18}O$ value ($\delta^{18}O = 2.78‰$), which falls within the range of available $\delta^{18}O$ data in cassiterite ($\delta^{18}O = 1.6-3.3‰$) and wolframite ($\delta^{18}O = 0.6-1.6‰$) from Rondônia Intrusive Suite (*e.g.*, Souza & Botelho 2009, Nascimento & Souza 2017). Lowered $\delta^{18}O$ values ($\delta^{18}O < 5‰$) in cassiterite and wolframite have been attributed to their greater susceptibility to isotopic fractionation during the rise of the hydrothermal-magmatic system and temperature drop (Kelly & Rye 1979, Sun & Eadington 1987, Zhang *et al.* 1994, Macey & Harris 2006, Li *et al.* 2022). However, the chemical variations, zoning, intergrowth, and micro-inclusions commonly found in these minerals may also interfere, to some degree, with the accuracy of isotopic measurements. In contrast, the available $\delta^{18}O$ data in quartz from the Rondônia Intrusive Suite often record higher $\delta^{18}O$ values ($\delta^{18}O = 9.3-11.8‰$; *e.g.*, Sparrenberger 2003, Souza & Botelho 2009; Santos Jr. 2015, Nascimento & Souza 2017). These higher values have been attributed to the low sensitivity of quartz to isotopic fractionation in the hydrothermal-magmatic system (Clayton *et al.* 1972, Taylor Jr. 1997, Sharp *et al.* 2016).

As the isotopic fractionation is temperature-dependent (Faure 1986, Hoefs 1997), $\delta^{18}O$ data obtained in

cassiterite-quartz-wolframite mineral pairs with paragenetic association have been commonly used as geothermometric parameters (*e.g.*, Zhang *et al.* 1994, Hu *et al.* 2005, Polyakov *et al.* 2005, Li *et al.* 2022). Geothermometric studies applying $\delta^{18}O$ data from Rondônia Intrusive Suite point to the following isotopic equilibrium temperature ranges: cassiterite-quartz = 495–415°C and wolframite-quartz = 433–309°C (Souza & Botelho 2009; Nascimento & Souza 2017). Although there is no reference curve for $\delta^{18}O$ isotopic fractionation of the quartz-columbite mineral pair, the similar $\delta^{18}O$ values between Cachoeirinha columbite-(Fe) and cassiterite may be used as geothermometric reference. Furthermore, the columbite-(Fe) + cassiterite association is commonly found in the primary ore sites of the Rondônia Intrusive Suite. Therefore, we consider the range between 400 and 500°C as reasonable for the isotopic fractionation temperature of the Cachoeirinha columbite-(Fe).

The geochronology of the polymetallic deposits of the Rondônia Tin Province indicates that the mineralization is related to late to post-magmatic hydrothermal phase with timing very close to magmatic crystallization ages (*e.g.*, Priem *et al.* 1971, Leite Jr. *et al.* 2001, Bettencourt *et al.* 2005, Souza *et al.* 2005, Santos Jr. 2015, Nascimento & Souza 2017). The Cachoeirinha Sn ± (Nb-Ta) alluvial deposit is inserted in the Rondônia Intrusive Suite (995–956 Ma), which hosts the main primary polymetallic deposits of the Rondônia Tin Province (Bettencourt *et al.* 1999, CPRM 2007). The U-Pb analytical results on Cachoeirinha CGM grains indicate the existence of two magmatic pulses that are responsible for the formation of ore deposits found in the alluvial sites—an older magmatic pulse with age 1052 ± 6 Ma followed by a younger magmatic pulse with age 909 ± 7 Ma. However, no particular petrographic features of these grains (*e.g.*, size, internal zoning, intergrowths, and micro-inclusions) were observed in an attempt to separate them. It is important to state that both ages might be slightly underestimated due to matrix effects related to the matrix-unmatched approach used. In addition, the LA-ICP-MS analysis also points to two generations of Cachoeirinha CGM grains, mainly marked by variations in $MREE_N$ and $HREE_N$ content. Despite some uncertainty, the results suggest that the younger magmatic pulse is relatively enriched in $MREE_N$ and $HREE_N$, indicating a greater degree of fractionation during the final stages of magmatic evolution (Graupner *et al.* 2010).

The Meso- to Neoproterozoic late-stage rapakivi magmatism in the Rondônia Tin Province has polyphasic characteristics, which incorporate various Sn ± (W, Nb-Ta)-specialized pulses (Bettencourt *et al.* 1999, 2005). Therefore, it is reasonable to propose that at least two magmatic pulses can be suggested as the sources of ore for the alluvial deposits of the polyphasic Cachoeirinha massif.

CONCLUSION

The Cachoeirinha CGM have mainly columbite-(Fe) composition, whose the (apfu)-general formula is $A(Fe_{0.552-0.979} - Mn_{0.095-0.414})$ $B(Ta_{0.042-0.551} - Nb_{1.305-1.871})_2O_6$. It still exhibits diverse internal zoning from the edges to the core, which is caused by ionic substitutions and resorption mechanisms

between Nb-rich and Ta-rich phases (Nb ↔ Ta) in the *B*-site. This mechanism is primarily controlled by oscillations in pH and fO_2 conditions during the temperature decreases. At the same time, complex coupled substitutions also occurred in the octahedral *A*- and *B*-sites, which allowed the entry of Sn and Ti ions, as well as other geochemical impurities (Ba, Cr, V, W, and U). The coupled substitution mechanisms can be represented by the following general equation: $3(Sn, Ti, U, Si)^{4+} + (W, Cr)^{6+} \leftrightarrow 2(V, Nb, Ta)^{5+} + 2(Al, REE)^{3+} + (Fe, Mn, Ba)^{2+}$.

The Cachoeirinha CGM has a low oxygen isotope value ($\delta^{18}O = 2.78$ ‰), which is consistent with the isotopic data available on cassiterite ($\delta^{18}O = 1.6$–3.3‰) and wolframite ($\delta^{18}O = 0.6$–1.6‰) from magmatic pulse related to the Rondônia Intrusive Suite. This isotopic characteristic confirms the greater susceptibility of these ore minerals to isotopic fractionation during temperature drop linked to a hybrid hydrothermal-magmatic system with low oxygen isotope value ($\delta^{18}O < 5$‰). The columbite-(Fe) + cassiterite paragenetic association is common in the primary ores of the Rondônia Intrusive Suite, which have a crystallization temperature range between 400 and 500°C.

The Cachoeirinha CGM U-Pb geochronological investigation revealed that the Cachoeirinha alluvial deposit hosts mineralization (columbite-(Fe) + cassiterite) related to at least two Neo-Mesoproterozoic magmatic pulses. An older magmatic pulse occurred approximately 1052 ± 6 Ma, followed by a younger magmatic pulse around 909 ± 7 Ma. The Cachoeirinha CGM grains related to younger magmatic pulse tend to be relatively enriched in $MREE_N$ and $HREE_N$, indicating a greater degree of fractionation.

ACKNOWLEDGMENTS

REFERENCES

Abdalla H.M., Helba H.A., Mohamed F.H. 1998. Chemistry of columbite-tantalite minerals in rare metal granitoids, Eastern Desert, Egypt. *Mineralogical Magazine*, **62**(6):821-836.

Alderton D.H.M. 1989. Oxygen isotope fractionation between cassiterite and water. *Mineralogical Magazine*, **53**(371):373-376.

Anderson M.O., Lentz D.R., Mcfarlane C.R.M., Falck H. 2013. A geological, geochemical and textural study of a LCT pegmatite: implications for the magmatic versus metasomatic origin of Nb–Ta mineralization in the Moose II pegmatite, Northwest Territories, Canada. *Journal of Geosciences*, **58**(4):299-320. https://doi.org/10.3190/jgeosci.149

ANM. 2020. *Anuário Mineral Brasileiro: Principais Substâncias Metálicas*. Brasília: ANM. Available at: https://dados.gov.br/dataset/anuario-mineral-brasileiro-amb. Accessed on: Mar. 16th, 2021.

Badanina E.V., Sitnikova M.A., Gordienko V.V., Melcher F., Gäbler H.-E., Lodziak J., Syritso L.F. 2015. Mineral chemistry of columbite–tantalite from spodumene pegmatites of Kolmozero, Kola Peninsula (Russia). *Ore Geology Reviews*, **64**:720-735. https://doi.org/10.1016/j.oregeorev.2014.05.009

Bartels A., Holtz F., Linnen R.L. 2010. Solubility of manganotantalite and manganocolumbite in pegmatitic melts. *American Mineralogist*, **95**(4):537-544. https://doi.org/10.2138/am.2010.3157

Bettencourt J.S., Leite Jr. W.B., Goraieb C.L., Sparrenberger I., Bello R.M.S., Payolla B.L. 2005. Sn-polymetallic greisen-type deposits associated with late-stage rapakivi granites, Brazil: Fluid inclusion and stable isotope characteristics. *Lithos*, **80**(1-4):363-386. https://doi.org/10.1016/j.lithos.2004.03.060

Bettencourt J.S., Leite Jr. W.B., Ruiz A.S., Matos R., Payolla B.L., Tosdal R.M. 2010. The Rondonian-San Ignacio Province in the SW Amazonian Craton: An overview. *Journal of South American Earth Sciences*, **29**(1):28-46. https://doi.org/10.1016/j.jsames.2009.08.006

Bettencourt J.S., Muzzolon R., Payolla B.L., Dall'Ígna L.G., Pinho O.D. 1988. Depósitos estaníferos secundários da região central de Rondônia. In: Schobbenhaus C., Coelho C.E.S. (Coord.). *Principais Depósitos Minerais do Brasil:* Metais básicos não ferrosos, ouro e alumínio. Brasília: MME/DNPM/Vale do Rio Doce. v. III. p. 213-241.

Bettencourt J.S., Tosdal R.M., Leite Jr. W.B., Payolla B.L. 1999. Mesoproterozoic rapakivi granites of the Rondônia Tin Province, southwestern border of the Amazonian craton, Brazil – I. Reconnaissance U-Pb geochronology and regional implications. *Precambrian Research*, **95**(1-2):41-67. https://doi.org/10.1016/S0301-9268(98)00126-0

Breiter K., Korbelová Z., Chládek Š., Uher P., Knesl I., Rambousek P., Honig S., Šešulka V. 2017. Diversity of Ti–Sn–W–Nb–Ta oxide minerals in the classic granite-related magmatic–hydrothermal Cínovec/Zinnwald Sn–W–Li deposit (Czech Republic). *European Journal of Mineralogy*, **29**(4):727-738. https://doi.org/10.1127/ejm/2017/0029-2650

Černý P., Blevin M., Cuney M., London D. 2005. Granite-related ore deposits. *Economic Geology*, 100th Anniversary Volume, paper 11, 337-370. https://doi.org/10.5382/AV100.12

Černý P. & Ercit T.S. 1989. Mineralogy of niobium and tantalum: crystal chemical relationships, paragenetic aspects and their economic implications. In: Moller P., Černý P., Saupe F. (Eds.). *Lanthanides, Tantalum and Niobium*. Special Publication No. 7 of the Society for Geology Applied to Mineral Deposits. Berlin: Springer. Part 1. p. 27-79.

Černý P., Goad B.E., Hawthorne F.C., Chapman R. 1986. Fractionation trends of the Nb-Ta and Ta-bearing oxide minerals in the Greer Lake pegmatitic granite and its pegmatite aureole, southeastern Manitoba. *American Mineralogist*, **71**(3-4):501-517.

Černý P., Meintzer R.E., Anderson A.J. 1985. Extreme fractionation in rare-element granitic pegmatites; selected examples of data and mechanisms. *The Canadian Mineralogist*, **23**(3):381-421.

Che X.D., Wu F.Y., Wang R.C., Gerdes A., Ji W.Q., Zhao Z.H., Yang J.H., Zhu Z.Y. 2015. In situ U–Pb isotopic dating of columbite–tantalite by LA–ICP–MS. *Ore Geology Reviews*, **65**(Part 4):979-989. https://doi.org/10.1016/j.oregeorev.2014.07.008

Chen L.L., Ni P., Li W.S., Ding J.Y., Pan J.Y., Wang G.G., Yang Y.L. 2018. The link between fluid evolution and vertical zonation at the Maoping tungsten deposit, Southern Jiangxi, China: Fluid inclusion and stable isotope evidence. *Journal of Geochemical Exploration*, **192**:18-32. https://doi.org/10.1016/j.gexplo.2018.01.001

Chevychelov V.Y., Borodulin G.P., Zaraisky G.P. 2010. Solubility of columbite, (Mn, Fe)(Nb, Ta)2O6, in granitoid and alkaline melts at 650–850°C and 30–400MPa: an experimental investigation. *Geochemistry International*, **48**(5):456-464. https://doi.org/10.1134/S0016702910050034

Chudík P., Uher P., Kohút M., Bačík P. 2008. Accessory columbite to tantalite, tapiolite and zircon: products of extreme fractionation in highly peraluminous pegmatitic granite from the Považský Inovec Mountains, Western Carpathians, Slovaki. *Journal of Geosciences*, **53**(4):323-334. https://doi.org/10.3190/jgeosci.031

Clayton R.N. & Mayeda T.K. 1963. The use of bromine pentafluoride in the extraction of oxygen from oxides and silicates for isotopic analysis. *Geochimica et Cosmochimica Acta*, **27**(1):43-52. https://doi.org/10.1016/0016-7037(63)90071-1

Clayton R.N., O'Neil J.R., Mayeda T.K. 1972. Oxygen isotope exchange between quartz and water. *Journal of Geophysical Research*, **77**(17):3057-3067. https://doi.org/10.1029/JB077i017p03057

CPRM. 2007. *Geologia e recursos minerais do Estado de Rondônia: Sistema de Informações Geográficas - SIG*. Texto Explicativo do Mapa Geológico e de Recursos Minerais do Estado de Rondônia - Escala 1:1.000.000. Porto Velho: CPRM. CD-ROM.

Dall'Igna L.G. 1996. A mineração e o garimpo de cassiterite em Rondônia. *A Terra em Revista*, **2**(1):56-61.

Dall'Igna L.G. & Adamy A. 2010. Recursos minerais. In: Adamy A. (ed.). *Geodiversidade do Estado de Rondônia*. Programa Geologia do Brasil. Porto Velho: MME/CPRM. p. 121-132.

Faure G. 1986. *Principles of isotopic geology*. 2nd ed. New York: John Wiley & Sons.

Gonçalves G.O., Lana C., Scholz R., Buick I.S., Gerdes A., Kamo S.L., Corfu F., Rubatto D., Wiedenbeck M., Nalini Jr. H.A., Oliveira L.C.A. 2018. The Diamantina monazite: A new low-Th reference material for microanalysis. *Geostandards and Geoanalytical Research*, **42**(1):25-47. https://doi.org/10.1111/ggr.12192

González T.L., Polonio F.G., Moro F.J.L., Fernández A.F., Contreras J L.S., Benito M.C.M. 2017. Tin-tantalum-niobium mineralization in the Penouta deposit (NW Spain): Textural features and mineral chemistry to unravel the genesis and evolution of cassiterite and columbite group minerals in a peraluminous system. *Ore Geology Reviews*, **81**(Part 1):79-95. https://doi.org/10.1016/j.oregeorev.2016.10.034

Graupner T., Melcher F., Gäbler H.-E., Sitnikova M., Brätz H. Bahr A. 2010. Rare earth element geochemistry of columbite-group minerals: LA-ICP-MS data. *Mineralogical Magazine*, 74(4):691–713. https://doi.org/10.1180/minmag.2010.074.4.691

Hannah J.L. & Stein H.J. 1990. Magmatic and hydrothermal processes in ore-bearing systems. In: Stein H. & Hannah J. (Eds.) *Ore-bearing Granite Systems: Petrogenesis and Mineralizing Processes*. Geological Society of America, Special Papers 246. p. 1-11.

Heinrich C.A. 1990. The chemistry of hydrothermal tin(-tungsten) ore deposition. *Economic Geology*, **85**(3):457-481. https://doi.org/10.2113/gsecongeo.85.3.457

Heinrich C.A., Walshe J.L., Harrold B.P. 1996. Chemical mass transfer modelling of ore-forming hydrothermal systems: Current practice and problems. *Ore Geology Reviews*, **10**(3-6):319-338.

Hoefs J. 1997. *Stable Isotope Geochemistry*. New York: Springer-Verlag. https://doi.org/10.1007/978-3-662-03377-7

Horstwood M.S.A., Kosler J., Gehrels G., Jackson S.E., McLean N.M., Paton C., Pearson N.J., Sircombe K., Sylvester P., Vermeesch P., Bowring J.F., Condon D.J., Schoene B. 2016. Community-derived standards for LA-ICP-MS U-(Th-)Pb geochronology–uncertainty propagation, age interpretation and data reporting. *Geostandards and Geoanalytical Research*, **40**(3):311-332. https://doi.org/10.1111/j.1751-908X.2016.00379.x

Hu G., Clayton R.N., Polyakov V.B., Mineev S.D. 2005. Oxygen isotope fractionation factors involving cassiterite (SnO_2): II. Determination by direct isotope exchange between cassiterite and calcite. *Geochimica et Cosmochimica Acta*, **69**(5):1301-1305. https://doi.org/10.1016/j.gca.2004.09.002

Isotta C.A.L., Carneiro J.M., Kato H.T., Barros R.J.L. 1978. *Projeto Província Estanífera de Rondônia: relatório final*. Porto Velho: MME/DNPM/CPRM. v. 1.

Jackson K.J. & Helgeson H.C. 1985. Chemical and thermodynamic constraints on the hydrothermal transport and deposition of tin: I. Calculation of the solubility of cassiterite at high pressures and temperatures. *Geochimica et Cosmochimica Acta*, **49**(1):1-22. https://doi.org/10.1016/0016-7037(85)90187-5

Jackson S.E., Pearson N.J., Griffin W.L., Belousova E.A. 2004. The application of laser ablation-inductively coupled plasma-mass spectrometry to in situ U–Pb zircon geochronology. *Chemical Geology*, **211**(1-2):47-69. https://doi.org/10.1016/j.chemgeo.2004.06.017

Jaffey A.H., Flynn K.F., Glendenin L. E., Bentley W.C., Essling A.M. 1971. Precision measurement of half-lives and specific activities of [235]U and [238]U. *Physical Review C*, **4**(5):1889-1906. https://doi.org/10.1103/PhysRevC.4.1889

Jochum K.P., Weis U., Schwager B., Stoll B., Wilson S.A., Haug G.H., Andreae M.O., Enzweiler J. 2016. Reference values following ISO guidelines for frequently requested rock reference materials. *Geostandards and Geoanalytical Research*, **40**(3):333-350. https://doi.org/10.1111/j.1751-908X.2015.00392.x

Kelly W.C. & Rye R.O. 1979. Geologic, fluid inclusion, and stable isotope studies of the tin-tungsten deposits of Panasqueira, Portugal. *Economic Geology*, **74**(8):1721-1822. https://doi.org/10.2113/gsecongeo.74.8.1721

Kloosterman J.B. 1966. Granites and rhyolites of S. Lourenço: a volcano-plutonic complex in southern Amazonia. *Revista de Engenharia, Mineração e Metalurgia*, **44**(262):169-171.

Kloosterman J.B. 1967. Ring-structures in the Oriente and Massangana granite complexes, Rondônia, Brazil. *Revista de Engenharia, Mineração e Metalurgia*, **45**(266):72-77.

Kloosterman J.B. 1968. Uma província do tipo nigeriano no sul da Amazônia. *Revista de Engenharia, Mineração e Metalurgia*, **47**(278):59-64; **47**(280):167-168.

Lahti S.I. 1987. Zoning in columbite-tantalite crystals from the granitic pegmatites of the Eräjärvi area, southern Finland. *Geochimica et Cosmochimica Acta*, **51**(3):509-517. https://doi.org/10.1016/0016-7037(87)90065-2

Leal J.W.L., Silva G.H., Santos D.B., Teixeira W., Lima M.I.C., Fernandes C.A.C., Pinto A.C. 1978. *Levantamento de Recursos Naturais*: Folha SC.20 Porto Velho (I – Geologia). Projeto RADAMBRASIL. Rio de Janeiro: MME/DNPM. v. 16.

Legros H., Mercadier J., Villeneuve J., Romer R.L., Deloule E., Van Lichtervelde M., Dewaele S., Lach P., Che X.D., Wang R.C., Zhu Z.Y., Gloaguen E., Melleton J. 2019. U-Pb isotopic dating of columbite-tantalite minerals: Development of reference materials and in situ applications by ion microprobe. *Chemical Geology*, **512**:69-84. https://doi.org/10.1016/j.chemgeo.2019.03.001

Leite Jr. W.B. 2002. *A Suíte Intrusiva Santa Clara (RO) e a mineralização primária polimetálica (Sn,W, Nb, Ta, Zn, Cu e Pb) associada*. Tese de Doutorado, Instituto de Geociências, Universidade de São Paulo, São Paulo, 247 p.

Leite Jr. W.B., Payolla B.L., Betttencourt J.S., Tassinari C.C.G. 2001. New K-Ar ages of the primary tin mineralization in the Rondônia Tin Province, Brazil. *In*: III South American Symposium on Isotope Geology (SSAGI), Pucon-Chile, **5**:484-487. CD-ROM.

Li Y., He S., Zhang R.-Q., Bi X.-W., Feng L.-J., Tang G.-Q., Wang W.-Z., Huang F., Li X.-H., 2022. Cassiterite oxygen isotopes in magmatic-hydrothermal systems: in situ microanalysis, fractionation factor, and applications. *Mineralium Deposita*, **57**:643-661. https://doi.org/10.1007/s00126-021-01068-x

Lichtervelde M.V., Salvi S., Beziat D. 2007. Textural Features and Chemical Evolution in Tantalum Oxides: Magmatic Versus Hydrothermal Origins for Ta Mineralization in the Tanco Lower Pegmatite, Manitoba, Canada. *Economic Geology*, **102**(2):257-276. https://doi.org/10.2113/gsecongeo.102.2.257

Linnen R.L. & Keppler H. 1997. Columbite solubility in granitic melts: consequences for the enrichment and fractionation of Nb and Ta in the Earth's crust. *Contributions to Mineralogy and Petrology*, **128**(2):213-227. https://doi.org/10.1007/s004100050304

Macey P. & Harris C. 2006. Stable isotope and fluid inclusion evidence for the origin of the Brandberg West area Sn–W vein deposits, NW Namibia. *Mineralium Deposita*, **41**:671-690. https://doi.org/10.1007/s00126-006-0079-1

McDonough W.F. & Sun S.-S. 1995. Composition of the Earth. *Chemical Geology*, **120**(3-4):223-253. https://doi.org/10.1016/0009-2541(94)00140-4

Melcher F., Graupner T., Gäbler H.E., Sitnikova M., Henjes-Kunst F., Oberthür T., Gerdes A., Dewaele S. 2015. Tantalum–(niobium–tin) mineralization in African pegmatites and rare metal granites: constraints from Ta–Nb oxide mineralogy, geochemistry and U–Pb geochronology. *Ore Geology Reviews*, **64**:667-719. https://doi.org/10.1016/j.oregeorev.2013.09.003

Melcher F., Graupner T., Gäbler H-E., Sitnikova M., Oberthür T., Gerdes A., Badanina E., Chudy T. 2017. Mineralogical and chemical evolution of tantalum–(niobium–tin) mineralization in pegmatites and granites. Part 2: Worldwide examples (excluding Africa) and an overview of global metallogenetic patterns. *Ore Geology Reviews*, **89**:946-987. https://doi.org/10.1016/j.oregeorev.2016.03.014

Möller P., Dulski P., Szacki W., Malow G., Riedel E. 1988. Substitution of tin in cassiterite by tantalum, niobium, tungsten, iron and manganese. *Geochimica et Cosmochimica Acta*, **52**(6):1497-1503. https://doi.org/10.1016/0016-7037(88)90220-7

Moon S.H., Park H.I., Ripley E.M., Lee I. 1996. Mineralogic and stable isotope studies of cassiterite greisen mineralization in the Uljin area, Korea. *Economic Geology*, **91**(5):916-933. https://doi.org/10.2113/gsecongeo.91.5.916

Nascimento T.M.F. & Souza V.S. 2017. Mineralogy, stable isotopes (δ^{18}O and δ^{34}S) and ^{40}Ar-^{39}Ar geochronology studies on the hydrothermal carapace of the Igarapé Manteiga W-Sn Deposit, Rondônia. *Brazilian Journal of Geology*, **47**(4):591-613. https://doi.org/10.1590/2317-4889201720170068

Neiva A.M.R. 1996. Geochemistry of cassiterite and its inclusions and exsolutions products from tin and tungsten deposits in Portugal. *The Canadian Mineralogist*, **34**(4):745-768.

Neiva A.M.R. 2008. Geochemistry of cassiterite and wolframite from tin and tungsten quartz veins in Portugal. *Ore Geology Reviews*, **33**(3-4):221-238. https://doi.org/10.1016/j.oregeorev.2006.05.013

Neiva A.M., Gomes C.L., Silva P.B., 2015. Two generations of zoned crystals of columbite-group minerals from granitic aplite–pegmatite in the Gouveia area, central Portugal. *European Journal of Mineralogy*, **27**(6): 771-782.

Oliveira S.M.B. & Valente J.C.P. 1993. Contribuição à metalogênese do estanho em meio supergênico – a jazida da onça B em Rondônia. *Revista Brasileira de Geociências*, **23**(4):400-407.

Paton C., Hellstrom J., Paul B., Woodhead J., Hergtb J. 2011. Iolite: Freeware for the visualisation and processing of mass spectrometric data.

Journal of Analytical Atomic Spectrometry, **26**(12):2508-2518. https://doi.org/10.1039/c1ja10172b

Payolla B.L. Bettencourt J.S., Kozuch M., Leite Jr. W.B., Fetter A.H., Van Schmus W.R. 2002. Geological evolution of the basement rocks in the east-central part of the Rondônia Tin Province, SW Amazonian Craton, Brazil: U-Pb and Sm-Nd isotopic constraints. *Precambrian Research*, **119**(1-4):141-169. https://doi.org/10.1016/S0301-9268(02)00121-3

Petrus J.A. & Kamber B.S. 2012. VizualAge: A novel approach to laser ablation ICP-MS U-Pb geochronology data reduction. *Geostandards and Geoanalytical Research*, **36**(3):247-270. https://doi.org/10.1111/j.1751-908X.2012.00158.x

Polyakov V.B., Mineev S.D., Clayton R.N., Hu G., Gurevich V.M., Khramov D.A., Gavrichev K.S., Gorbunov V.E., Golushina L.N. 2005. Oxygen isotope fractionation factors involving cassiterite (SnO_2): I. Calculation of reduced partition function ratios from heat capacity and X-ray resonant studies. *Geochimica et Cosmochimica Acta*, **69**(5):1287-1300. https://doi.org/10.1016/j.gca.2004.08.034

Priem H.N.A., Boelrijk N.A.I.M., Hebeda E.H., Verdurmen E.A.Th., Verschure R.H., Bon E.H. 1971. Granitic complexes and associated tin mineralizations of "Grenville" age in Rondônia, Western Brazil. *Geological Society of America Bulletin*, **82**(4):1095-1102. https://doi.org/10.1130/0016-7606(1971)82[1095:GCAATM]2.0.CO;2

Raimbault L., Cuney M., Azencott C., Duthou J.L., Joron J.L. 1995. Geochemical evidence for a multistage magmatic genesis of Ta-Sn-Li mineralization in the granite at Beauvoir, French Massif Central. *Economic Geology*, **90**(3):548-576. https://doi.org/10.2113/gsecongeo.90.3.548

Santos J.O.S., Rizzotto G.J., Potter P.E., McNaughton N.J., Matos R.S., Hartmann L.A., Chemale Jr. F., Quadros M.E.S. 2008. Age and autochthonous evolution of the Sunsás Orogen in West Amazon Craton based on mapping and U–Pb geochronology. *Precambrian Research*, **165**(3-4):120-152. https://doi.org/10.1016/j.precamres.2008.06.009

Santos Jr. P.S.M. 2015. *Metalogênese do depósito estanífero Liberdade, Campo Novo de Rondônia – RO*. Dissertação de Mestrado, Instituto de Geociências, Universidade de Brasília, 87 p.

Scandolara J.E., Fuck R.A., Dantas E.L., Souza V.S. 2013. Geochemistry of Jamari Complex, central-eastern Rondônia: Andean type magmatic arc and Paleoproterozoic crustal growth of the southwestern Amazonian Craton, Brazil. *Journal of South American Earth Sciences*, **46**:35-62. https://doi.org/10.1016/j.jsames.2013.04.002

Sharp Z.D., Gibbons J.A., Maltsev O., Atudorei V., Pack A., Sengupta S., Shock E.L., Knauth L.P. 2016. A calibration of the triple oxygen isotope fractionation in the SiO_2-H_2O system and applications to natural samples. *Geochimica et Cosmochimica Acta*, **186**:105-119. https://doi.org/10.1016/j.gca.2016.04.047

Siachoque A., Garcia R., Vlach S.R. 2020. Occurrence and composition of columbite-(Fe) in the reduced A-Type Desemborque pluton, Graciosa Province (S-SE Brazil). *Minerals*, **10**(5):411. https://doi.org/10.3390/min10050411

Sláma J., Košler J., Condon D.J., Crowley J.L., Gerdes A., Hanchar J.M., Horstwood M.S.A., Morris G.A., Nasdala L., Norberg N., Schaltegger U., Schoene B., Tubrett M.N., Whitehouse M.J. 2008. Plešovice zircon: A new natural reference material for U-Pb and Hf isotopic microanalysis. *Chemical Geology*, **249**(1-2):1-35. https://doi.org/10.1016/j.chemgeo.2007.11.005

Souza E.C., Melo A.F.F., Adamy A., Soeiro R.S., Daleiro V. 1975. *Projeto Nordeste de Rondônia: Relatório Final*. Brasília: MME/DNPM/CPRM. v. 1.

Souza V.S. 2003. *Evolução magmática e modelo metalogenético do sistema vulcano-plutônico estanífero Bom Futuro (RO)*. Tese de Doutorado, Instituto de Geociências, Universidade de Brasília, Brasília, 240 p.

Souza V.S. & Botelho N.F. 2002. Geologia do depósito de estanho do Bom Futuro (Rondônia) e composição dos fluidos nos sistemas de veios e greisens. In: Klein E.L., Vasquez M.L., Rosa-Costa L.T. (Eds.). *Contribuições à Geologia da Amazônia*. Belém: SBG-NO. v. 3. p. 99-214.

Souza V.S. & Botelho N.F. 2009. Composição química e isótopos de oxigênio em cassiterita e wolframita nos greisens do albita granito Palanqueta, depósito de estanho de Bom Futuro (RO). *Revista Brasileira de Geociências*, **39**(4):695-704. https://doi.org/10.25249/0375-7536.2009394695704

Souza V.S., Teixeira L.M., Botelho N.F. 2005. Datação U-Th-Pb de monazita hidrotermal e sua aplicação na geocronologia da mineralização de estanho em zonas de greisen do sistema granítico Palanqueta, depósito de estanho do Bom Futuro (RO). *Revista Brasileira de Geociências*, **35**(1):43-48.

Souza V.S., Teixeira L.M., Dantas E.L. Botelho N.F., Laux J.H. 2006. Idades U-Th-Pb e U-Pb em monazita de ortognaisse do Complexo Jamari, área do depósito de estanho de Bom Futuro (RO). *Revista Brasileira de Geociências*, **36**(1):71-76. https://doi.org/10.25249/0375-7536.200636S17176

Sparrenberger I. 2003. *Evolução da mineralização primária estanífera associada ao maciço granítico Santa Bárbara, Rondônia*. Tese de Doutorado, Instituto de Geociências, Universidade de São Paulo, São Paulo, 252 p.

Sun S.S. & Eadington P.J. 1987. Oxygen isotope evidence for the mixing of magmatic and meteoric waters during tin mineralization in the Mole granite, New South Wales, Australia. *Economic Geology*, **82**(1):43-52. https://doi.org/10.2113/gsecongeo.82.1.43

Taylor Jr. H.P. 1997. Oxygen and hydrogen isotope relationships in hydrothermal mineral deposits. In: Barnes H.L. (Ed.). *Geochemistry of hydrothermal ore deposits*. 3rd ed. New York: John Wiley & Sons. p. 229-302.

Tindle A.C. & Breaks F.W. 2000. Columbite-tantalite mineral chemistry from rare-element granitic pegmatites: Separation Lake area, NW Ontario, Canada. *Mineralogy and Petrology*, **70**:165-198. https://doi.org/10.1007/s007100070002

Uher P., Černý P., Chapman R., Határ J., Miko O. 1998. Evolution of Nb,Ta-Oxide minerals in the Prasivá Granitic Pegmatites, Slovakia. II. external hydrothermal Pb,Sb overprint. *The Canadian Mineralogist*, **36**(2):535-545.

Veiga A.T.C. 1990. *Significado paleo-ambiental e econômico dos aluviões auríferos e estaníferos da Amazônia*. Instituto de Geociências, Universidade de Brasília, Dissertação de Mestrado, Brasília, 111 p.

Veiga A.T.C., Dardenne M.A., Salomão E.P. 1988. Geologia dos aluviões auríferos e estaníferos da Amazônia. *In*: Anais do 35º Congresso Brasileiro de Geologia, SBG, Belém, **1**:164-177.

Vho A, Lanari P, Rubatto D. 2019. An internally consistent database for oxygen isotope fractionation between minerals. *Journal of Petrology*, **60**(11):2101-2129. https://doi.org/10.1093/petrology/egaa001

Wang Y., Li J., Lu J., Fan W. 1982. Geochemical mechanism of Nb-Ta-mineralization during the late stage of granite crystallization. *Geochemistry*, **1**(2):175-185. https://doi.org/10.1007/BF03180328

Wenger M., Armbruster T., Geiger C.A. 1991. Cation distribution in partially ordered columbite from the Kings Mountain pegmatite, North Carolina. *American Mineralogist*, **76**(11-12):1897-1904.

Wiedenbeck M., Allé P., Corfu F., Griffin W.L., Meier M., Oberli F., Quadt A.V., Roddick J.C., Spiegel W. 1995. Three natural zircon standards for U-Th-Pb, Lu-Hf, trace element and REE analyses. *Geostandards Newsletter*, **19**(1):1-23. https://doi.org/10.1111/j.1751-908X.1995.tb00147.x

Wise M.A., Brown C.D. 2011. Chemical composition of coexisting columbite-group minerals and cassiterite from the Black Mountain pegmatite, Maine. *European Journal of Mineralogy*, **23**(5):817-828. https://doi.org/10.1127/0935-1221/2011/0023-2102

Wise M.A., Černý P., Falster A.U. 1998. Scandium substitution in columbite-group minerals and ixiolite. *The Canadian Mineralogist*, **36**(2):673-680.

Wise M.A., Francis C.A., Černý P. 2012. Compositional and structural variations in columbite-group minerals from granitic pegmatites of the Brunswick and Oxford fields, Maine: Differential trends in F-poor and F-rich environments. *Canadian Mineralogist*, **50**(6):1515-1530. https://doi.org/10.3749/canmin.50.6.1515

Wu F.-Y., Liu X.-C., Liu Z.-C., Wang R.-C., Xie L., Wang J.-M., Ji W.-Q., Yang L., Liu C., Khanal G.P., He S.-X. 2020. Highly fractionated Himalayan leucogranites and associated rare-metal mineralization. *Lithos*, **352-353**:105319. https://doi.org/10.1016/j.lithos.2019.105319

Yin R., Huang X.-L., Xu Y.-G., Wang R.-C., Wang H., Yuan C., Ma Q., Sun X.-M., Chen L.-L. 2020. Mineralogical constraints on the magmatic hydrothermal evolution of rare-elements deposits in the Bailongshan granitic pegmatites, Xinjiang, NW China. *Lithos*, **352-353**:105208. https://doi.org/10.1016/j.lithos.2019.105208

Yokoi O.Y., Viglio E.P., Waghorn J.G., Jones J.P., Figueroa L.A. 1987. Potosí, a primary tin deposit in Rondônia. *Revista Brasileira de Geociências*, **17**(4):557-561.

Zhang L.-G., Liu J.-X., Chen Z.-S., Zhou H.B. 1994. Experimental investigations of oxygen isotope fractionation in cassiterite and wolframite. *Economic Geology*, **89**(1):150-157. https://doi.org/10.2113/gsecongeo.89.1.150

Zheng Y.-F. 1991. Calculation of oxygen isotope fractionation in metal oxides. *Geochimica et Cosmochimica Acta*, **55**(8):2299-2307. https://doi.org/10.1016/0016-7037(91)90105-E